

Article

Load Frequency Control Using Demand Response and Storage Battery by Considering Renewable Energy Sources

Lei Liu ^{1,*} , Hidehito Matayoshi ¹, Mohammed Elsayed Lotfy ^{1,2} , Manoj Datta ³ and Tomonobu Senjyu ¹ 

¹ Department of Electrical and Electronics Engineering, University of the Ryukyus, Okinawa 903-0123, Japan; k178673@eve.u-ryukyu.ac.jp (H.M.); mohamedabozed@zu.edu.eg (M.E.L.); b985542@tec.u-ryukyu.ac.jp (T.S.)

² Department of Electrical Power and Machines, Zagazig University, Zagazig 44519, Egypt

³ Electrical and Computer Engineering School of Engineering, RMIT University, Melbourne 3000, Victoria, Australia; manoj.datta@rmit.edu.au

* Correspondence: k178557@eve.u-ryukyu.ac.jp; Tel.: +81-80-2957-2722

Received: 23 October 2018; Accepted: 3 December 2018; Published: 5 December 2018



Abstract: Renewable energy sources (RESs), as clean, abundant, and inexhaustible source of energy, have developed quickly in recent years and played more and more important roles around the world. However, RESs also have some disadvantages, such as the weakness of stability, and by the the estimated increase of utilizing RESs in the near future, researchers began to give more attention to these issues. This paper presents a novel output power fluctuate compensation scheme in the small-scale power system, verifying the effect of output power control using storage battery, demand response and RESs. Four scenarios are considered in the proposed approach: real-time pricing demand response employment, RESs output control use and both of demand response and RESs output control implementation. The performance of the proposed control technique is investigated using the real 10-bus power system model of Okinawa island, Japan. Moreover, the system stability is checked using the pole-zero maps for all of the control loops associated with the proposed scheme. The robustness and effectiveness of the proposed method was verified by simulation using Matlab[®]/Simulink[®].

Keywords: frequency control; renewable energy source; demand response; storage battery

1. Introduction

Even though diesel generators are still the most widely used resource around the world, they have several drawbacks: burning fossil fuel releases harmful emissions into the atmosphere and depletes the Earth's limited stored resources; this does not only affect the environment but also increases the cost of generating dramatically because of the need to purify harmful emissions and also, the transportation adds extra cost [1]. Due to the above factors, and by considering global warming and environment problems, renewable energy sources (RESs) have received more and more attention in recent years. RESs have many advantages: first, it is a clean source of energy, it means that it has low or zero carbon and greenhouse emission. Second, it is renewable, and it implies that they do not deplete over a lifetime and there is zeroes possibility that they will run out. RES also has much more advantages such as reliable, needs less maintenance of facilities and could stabilize the global energy prices, etc. Now, RES has many main forms such as solar power generation, wind generation, hydroelectric energy generation, biomass, hydrogen, fuel cell generation, and geothermal generation [2].

RES developed very fast in recent decades, even though it has many advantages but it also causes some problems, as their output power possesses stochastic and intermittent properties, so the RES have sharp fluctuations in their generated power due to weather conditions which lead to the supply-load mismatch that accordingly produce system frequency fluctuations [3]. Therefore, the output power of RES devices has to be controlled. Moreover, controlling RES's output power enables minimizing their influence on the power system. On the other hand, output control of RES still has a limit. One method to compensate for the load frequency fluctuation is by introducing energy storage devices. Energy storage devices can do important role in the traditional power systems as spinning reserve. Energy storage devices have the ability to balance between supply and demand, and accordingly maintain stability and improve power quality since RES are naturally intermittent. Energy storage devices can provide fast storage capacity with ability to share changes that happen in power requirements [4]. Another method to compensate for the load frequency fluctuation caused by the power imbalance between generation and load is demand response. Demand response can be defined as the capability to control loads by turning them on/off or even change their demand values depending on the situation with taking into consideration system security, power quality, and technical and economic constraints. Demand response has the ability to be the first option not last one for power systems frequency as recent studies shown. Moreover, due to ESS low efficient, high operation cost [5,6], and also high operation cost of generation side controllers [7], researchers gave more attention to demand response to improve power system security and reliability [8–10]. In addition, by using demand response, the generation side part in frequency control can be decrease and reduce the required amounts of spinning reserve, the operating costs, and CO₂ emissions too [11].

The frequency control approach in power systems has a long history, and there is plenty of related research. RES such as PV or wind fluctuations can negatively affect power system frequency. In recent years, several Battery Energy Storage Systems (BESS) were issued for peak shaving and load leveling [12,13]. Also, BESS has a faster dynamic response compared with other storage devices or even conventional generators due to its static structure. Reference [14] discusses BESS' potential for regulating frequency. Moreover [15] presents load frequency control approach using BESS in an isolated power system. Modern control techniques based on fixed state of charge (SOC) of BESS for large interconnected systems are developed in [16]. On the other hand, demand response can be consider as alternative remedy to mitigate the frequency fluctuations due to its fast dynamics [17]. Reference [18] discussed technical review on demand response and how to contribute it in power system frequency control. A frequency control scheme of smart appliances is shown in [19]. Moreover, frequency-time characteristics load [20,21], saturable reactors [22], and load control approach with electric vehicles [23] are considered as frequency-sensitive load controllers to investigate demand response contribution in frequency control of power systems.

Furthermore, References [24] investigate the effect of demand response with taking communication delay into consideration on frequency stability. Reference [25] discussed stochastic control scheme in which the duty cycle of domestic refrigerators can be adjusted as primary frequency control. The impact of controllable loads on the power system frequency is presented in [26]. Novel primary and secondary frequency reserves via multi-agent demand control for conventional generators are analyzed in [27]. Some works have been done in [28] considering demand response as spinning reserve. In addition, also a spinning reserve cooperation with demand response to restore frequency stability in case of contingencies is presented in [29]. Moreover, applying demand response as control reserve is proposed in [30]. Industrial pump loads, relay controllable loads, and programmable thermostats are used in [31] to regulate frequency in an island. Estimation process for demand and generation mismatch is discussed in [32] using minimum variance estimation technique with decentralized optimal load control approach.

There are also some other researchers who work on related research of load frequency control with RES. A new approach considering part of photovoltaic (PV) output power as back-up reserve for frequency control is analyze in [33]. Furthermore, integration of wind farm in power grid to control

frequency using droop control and inertia control techniques is proposed in [34]. Reference [35] presents the inclusion of plug-in electrical vehicles (PEVs) in microgrids. In [36], authors propose a full-order observer-based frequency control approach for a hybrid power system. In addition, another paper [37] proposes a control scheme in a small power system by implementing two decentralized fuzzy logic control (FLC)-based schemes.

Depending on the previous literature review, this paper proposes a novel load frequency control scheme using renewable energy sources and energy storage systems. Moreover, new control technique that combines maximum power point tracking approaches and output power control methods for photovoltaic and wind turbine generators is applied. Furthermore, price-based real-time pricing demand response is used with eight categories of controllable loads and its impact on frequency fluctuations suppression is investigated. Three case studies are considered using RES, storage battery, and real-time price demand response. In addition, fourth scenario with whole day simulation data is implemented to confirm the effectiveness and robustness of the proposed control approach. The performance of the intended scheme is investigated using the real 10-bus power system model of Okinawa island, Japan. Finally, all control loops related to the proposed control scheme are checked using pole-zero maps to confirm the power system stability.

The remaining of the paper is organized as follows: Section 2 presents the power system configuration used in this study. The applied Maximum Power Point Tracking techniques for PV and wind turbine are illustrated in Section 3. Section 4 clarifies the proposed output control scheme of renewable energy generation. The utilized real-time price demand response approach for suppressing frequency deviation is discussed in Section 5. Then Section 6 focuses on results. Detailed analysis and comparison between the four scenarios is then held in Section 7. Finally, Section 8 concludes the paper.

2. Power System Configuration

The real 10-bus power system model of Okinawa island, Japan is considered in this research as shown in Figure 1. Where G_x , WG_x , PV_x refer to thermal power generation, wind power generation and photovoltaic power generation, respectively. The parameters of thermal power generators are shown in Table 1 while its associated line admittances are presented in Table 2. Moreover, parameters of WG_x , PV_x and battery are discussed in Table 3. The excitation system using an automatic voltage regulator (AVR) is modeled by a first-order lag element as shown in Figure 2.

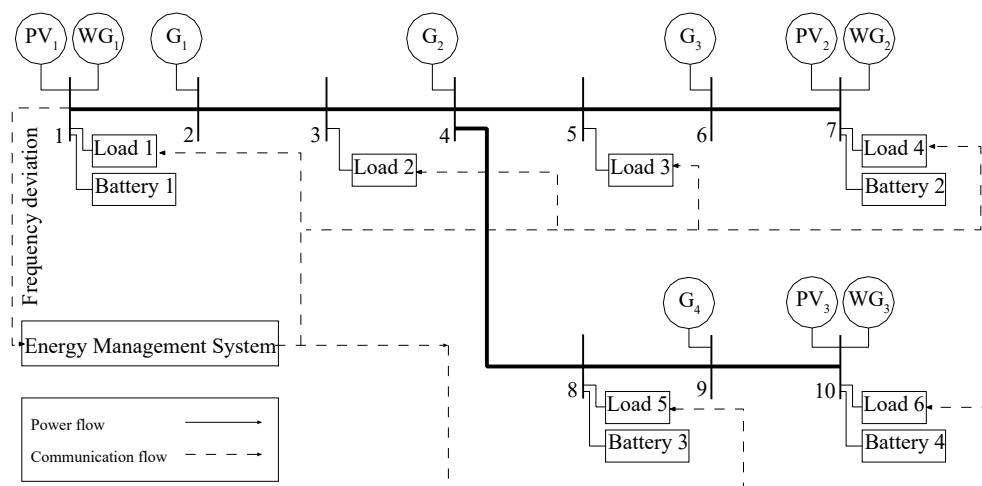


Figure 1. Power system model.

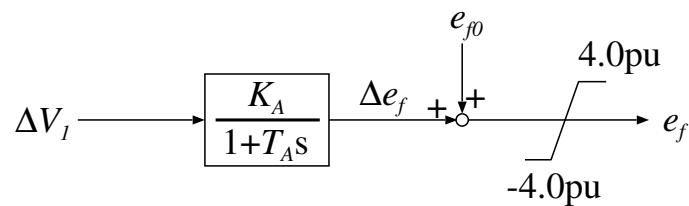


Figure 2. Automatic voltage regulator.

Table 1. Parameters of thermal power generators.

Gas-Turbine Generators	Unit	G ₁	G ₂	G ₃	G ₄
rated power	P_G [MW]	324	482	292	417
Inertia constant	H [s]	6.3	7.2	5.8	6.8
d-axis synchronous reactance	x_d [pu]	1.57	1.63	1.53	1.68
d-axis transient reactance	x'_d [pu]	0.261	0.268	0.298	0.312
q-axis synchronous reactance	x_q [pu]	1.06	0.98	1.12	0.98
q-axis transient reactance	x'_q [pu]	0.177	0.189	0.173	0.192
d-axis open-circuit transient time constant	T'_{d0} [s]	6.1	7.5	5.7	7.6
q-axis open-circuit transient time constant	T'_{q0} [s]	0.64	0.41	0.72	0.47
Amplifier gain	K_A	50	50	50	50
Amplifier time constant	T_A [s]	0.06	0.06	0.06	0.06
Governor time constant	T_G [s]	4.0	4.0	4.0	4.0

Table 2. Transmission line admittance.

Impedance	Unit	Value
line resistance	r [pu]	1.1048
line reactance	x [pu]	4.6954

Table 3. Parameters of each generators.

Wind-Turbine Generator	Unit	WG ₁	WG ₂	WG ₃	
Rated power	P_{wg} [MW]	10	7	8	
Photovoltaic Generator	Unit	PV ₁	PV ₂	PV ₃	
Rated power	P_{pv} [MW]	140	140	140	
Battery	Unit	1	2	3	4
Inverter capacity	[MVA]	25	25	25	25
Storage capacity	[MWh]	100	100	100	100

3. Load Frequency Control Using Maximum Power Point Tracking (MPPT) of Renewable Energy Generation

3.1. Maximum Power Point Tracking (MPPT) Control of PV Power Generation

This research adopted the hill climbing method as Maximum Power Point Tracking (MPPT) of PV power generation for its simplicity and robustness. Hill climbing determines PV output voltage command value by searching the PV output voltage to make the output of PV maximum, as shown in the characteristic curve (P-V curve) in Figure 3. At first, measure PV output voltage V_{pv} and PV output

power P_{pv} , compare with the value of V_{pv} and P_{pv} one step before, and then evaluate whether V_{pv} and P_{pv} are increasing or decreasing. Next, based on this information, determine the output voltage command value V_{pvmppt} , to find the maximum output power point. For MPPT control scheme used in this research, the sample time is 1 s, and the search time is 0.2 s, while the search intervals is 0.01 s. Moreover, the operation will work by maximum point explore in 0.8 s.

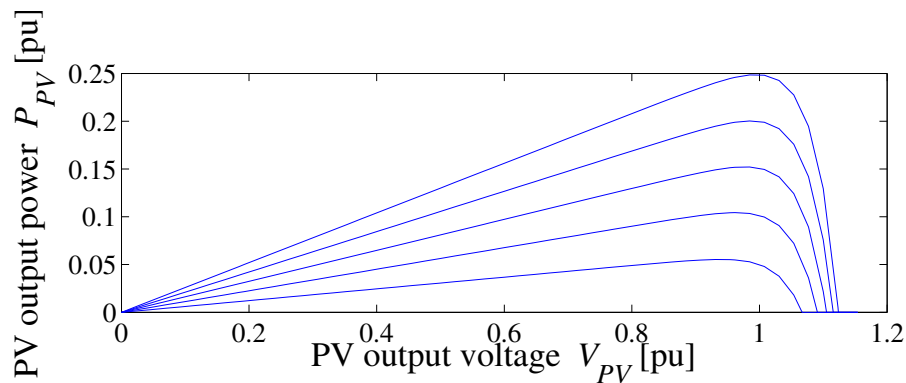


Figure 3. Output characteristics curve (P-V curve) of PV.

3.2. Maximum Power Point Tracking (MPPT) Control of Wind Turbine Generation

Wind output power MPPT is realized in this research by control the blade pitch. The output characteristics curve of Wind Generator (WG) corresponds to wind speed is shown in Figure 4. Wind turbine starts to generate power when wind speed exceeds cut-in speed. Then, in the interval between the cut-in speed and maximum speed, the blade pitch angle (β) is set to 0° deg to obtain the maximum power point. Next, when wind speed reaches the maximum speed, blade pitch control scheme tries to keep the output power at its rated value. When wind speed exceeds the cut-out value, pitch angle is set to 90° deg to shut-down the turbine for safety reasons. In this study cut-in, maximum and cut-out speeds are set to 5 m/s, 12 m/s, 25 m/s, respectively as shown in Figure 4.

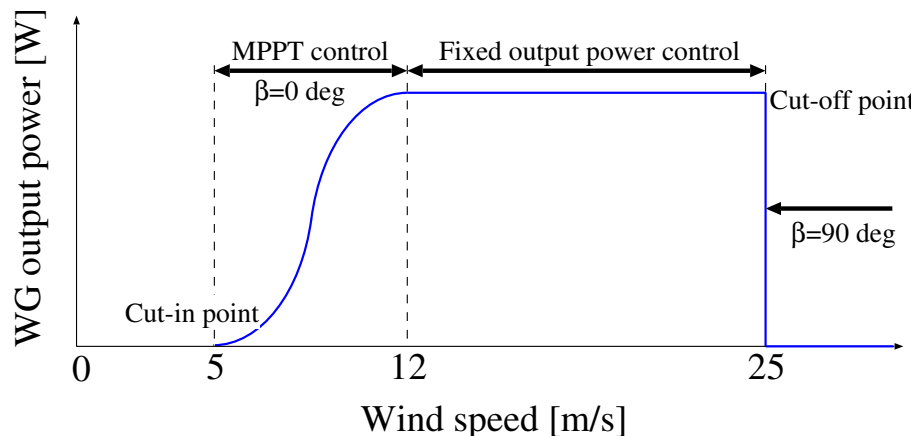


Figure 4. Output characteristics curve WG.

4. Output Control of Renewable Energy Generation

4.1. Output Control of Photovoltaic Generation (PV)

Photovoltaic generation output control is performed by adjusting the voltage of PV. Also, it can take the range of PV output voltage higher than the voltage that obtains maximum power. That is why damping control approach should be utilized to keep V_{pv} in the required value. The PV output suppression control system based on the frequency deviation is shown in Figure 5. PI control is used for frequency deviation control and terminal voltage command value of PV is determined by adding

the reference value. The PV output power is determined according to command terminal voltage value and P-V curves.

In this paper, as shown in Figure 6, by calculating the control weights from load frequency deviation amount, and based on the value of this control weight, the control method of renewable energy output can be decided. Generally, when system frequency exceeds 60 Hz, supply-demand balance becomes over-supplied, so it is necessary to decrease output of renewable energy generation. Therefore, suppression the output of renewable energy generation is limited at the case of frequency exceed 60 Hz or more. on the other hand, in the case of frequency at 60 Hz or less, it is performed by MPPT control. By adjusting the control weights of MPPT control and frequency control according to the frequency deviation amount, it can realize frequency fluctuation suppress.

$$k = 20 \cdot \Delta f \quad (0 \leq k \leq 1) \tag{1}$$

$$V_{PV} = kV_{PV_{ctrl}} + (1 - k)V_{PV_{MPPT}} \tag{2}$$

Here, The control weight k can be calculated by Equation (1), $0 \leq k \leq 1$ ($0 \leq \Delta f \leq 0.05$ Hz) (shown in Figure 7). When the amount of load frequency exceeds 60 Hz, k will increase, and the weight of the voltage command value of frequency control will increase. Conversely, when the system frequency close to 60 Hz, the value of k become smaller, and the MPPT control become accomplished. Voltage of PV could be calculated by Equation (2).

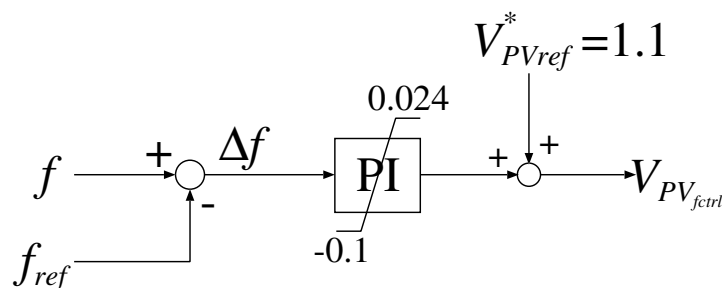


Figure 5. PV output suppression control system.

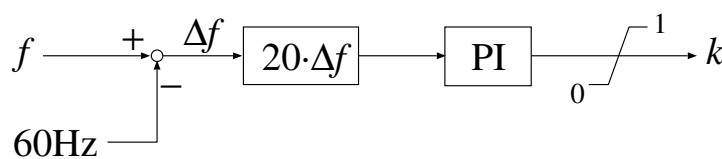


Figure 6. Block diagram of control weight.

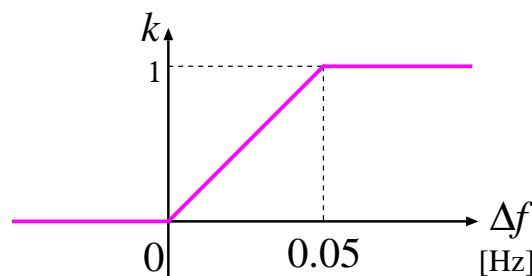


Figure 7. Control weight.

4.2. Output Control of Wind Turbine Generation

Output control of Wind generator(WG) is performed by changing the pitch angle of the blade. The pitch angle control system based on WG frequency control is shown in Figure 8. The hydraulic

servo system of pitch angle control system was simulated by a first-order lag transfer function with a time constant of 0.5 s. Similar to Photovoltaic generation (PV), based on control weight, when frequency fluctuation is small, power generation works according to Maximum Power Point Tracking(MPPT) control, when frequency fluctuation increase, it changed to load frequency control by considering pitch angle control. The control weights of MPPT control and frequency control are varied according to the frequency deviation, and frequency variation is suppressed by changing the control amount.

$$\beta = k\beta_{ctrl} + (1 - k)\beta_{MPPT} \tag{3}$$

Here, the pitch angle command value β could be calculated by Equation (3) at wind speed 5–25 m/s, and k is the same value as PV output control. As PV output control, the output of the wind generator can be controlled and control weight changes according to the deviation amount of system frequency.

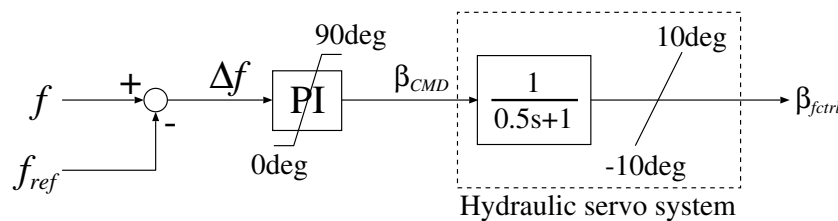


Figure 8. Pitch angle control system.

5. Demand-Response Control Scheme

5.1. Real-Time Pricing to Suppress Frequency Deviation

In this paper, real-time pricing demand response is utilized to modify the balance between supply and demand that changes from one moment to another, and accordingly causes the harmful frequency deviations. This goal is approached by varying the electricity price in real-time depending on the value of frequency deviation.

The model of price is presented in Figure 9. The relation between price and frequency deviation can be formulated as the following equation.

$$\pi^* = \frac{-0.3}{1 + \exp(-40 \cdot \Delta f)} + 0.35 \text{ [yen]} \tag{4}$$

where f , f_{ref} , π are power price, reference frequency (60 Hz), and frequency, respectively. Depending on the previous equation, the price of electricity will rise when frequency falls or if there is load increase to force the user to decrease his consumption. On the other hand, at the time of light load, electricity price will be reduced. So, the user can increase his consumption. First order lag filter that has time constant T_π is used to suppress high speed fluctuations of electricity price obtained by Equation (4). Moreover, the relation between frequency deviation and power price is shown in Figure 10.

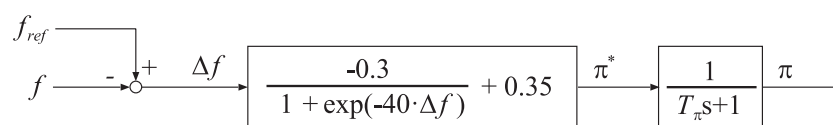


Figure 9. Configuration of pricing.

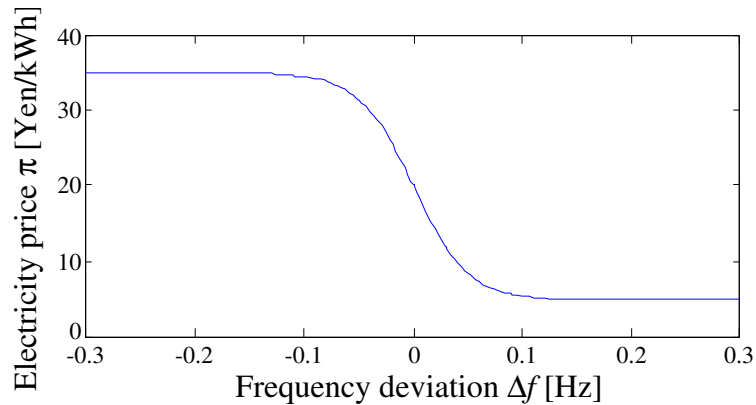


Figure 10. Electricity price π for frequency deviation Δf .

5.2. Auto Demand-Response

Eight kinds of loads are considered in this study and Figures 11 and 12 show their variations with electricity price. These loads can be categorized for 3 main types that can be described as follows:

- $P_{L1}, P_{L2}, P_{L3}, P_{L4}$: Continuously fluctuate with price fluctuations.
- P_{L5}, P_{L6} : These types of loads have hysteresis characteristics. In case of load 5, for example, the load will be 0 pu if electricity price reaches 30 yen and the load will be 0.155 pu for load 1, 2, 3, 5 and 0.311 pu for load 4, 6 if the electricity price reaches 25 yen.
- P_{L7}, P_{L8} : This type of load has hysteresis characteristic depending on rise or fall of consumption. So it can be considered as a load fluctuating stepwise.

The total power consumption of the load connected to the power system is considered to be 1400 MW. 600 MW is dealt as controllable load while the remaining part is considered as an uncontrollable one. The maximum power consumption for each load is indicated in Table 4, with clarifying the amount of controllable and uncontrollable loads.

Table 4. Maximum consumption power of each load.

Load	Type	Value
Load 1, 2, 3, 5	Uncontrollable load	100 MW
	Controllable load	75 MW
Load 4, 6	Uncontrollable load	200 MW
	Controllable load	150 MW
Total	Uncontrollable load	800 MW
	Controllable load	600 MW

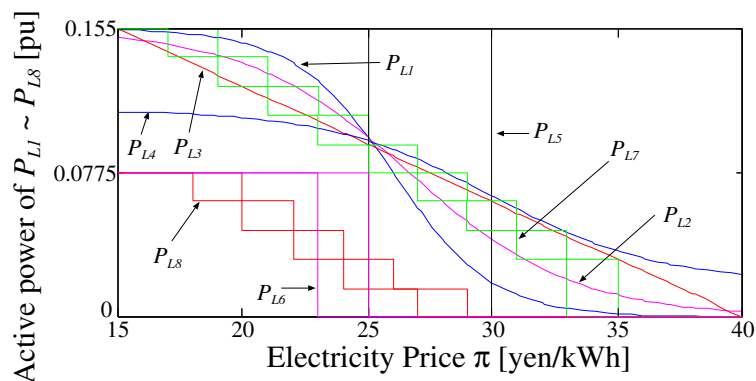


Figure 11. Power consumption of each controllable load for electricity price (Load 1, 2, 3, 5).

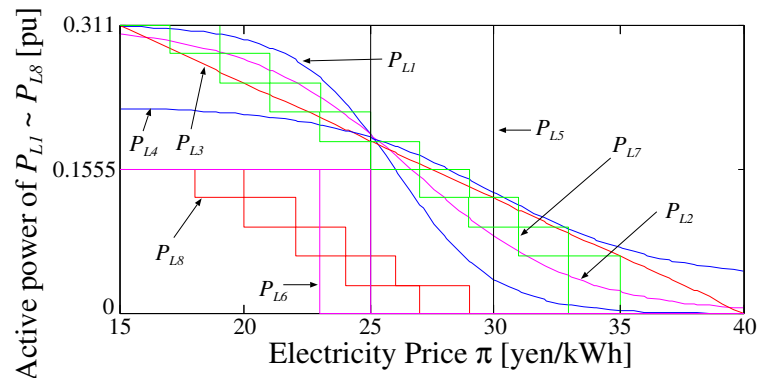


Figure 12. Power consumption of each controllable load for electricity price (Load 4, 6).

6. Results

Four case studies are implemented in this research. The first case which is considered the as base one consists of output control by the storage battery only. While the second, third, and fourth cases are using a storage battery with demand response, a storage battery with renewable energy generation control, and a storage battery with both of demand response and renewable energy generation output control, respectively. The connected renewable energy power generation is solar power generation and wind power generators, and the capacity of PV, which has remarkable growth in Japan recent years, is set to 420 MW ($140 \text{ MW} \times 3$ buses), the capacity of Wind turbine generators is set as 25 MW ($P_{wg1} = 10 \text{ MW}$, $P_{wg2} = 7 \text{ MW}$, $P_{wg3} = 8 \text{ MW}$). By the simulation condition, the solar radiation amount and the wind speed are shown in Figures 13 and 14. First, Figure 15 shows the simulation result of power control only with the storage battery, and Figure 16 represents power controlled by storage battery and demand response. Next, the result of power control by storage battery and renewable energy generation are shown in Figure 17, and the simulation results when demand response added into the above case are shown in Figure 18. Simulation results for installed capacities of battery is then presented in Figure 19, using supply power suppression of renewable energy source and demand response. Real whole day simulation data for wind speed and solar radiation of Okinawa, Japan are used and the associated simulation results of this case are then shown in Figure 20. Detailed analysis for the proposed scenarios are the shown in Section 7.

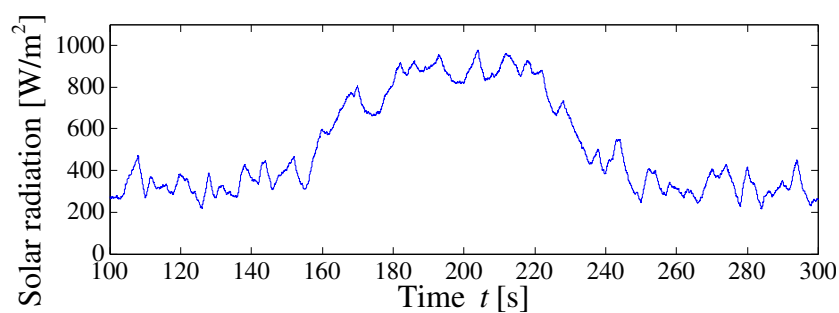


Figure 13. Solar radiation.

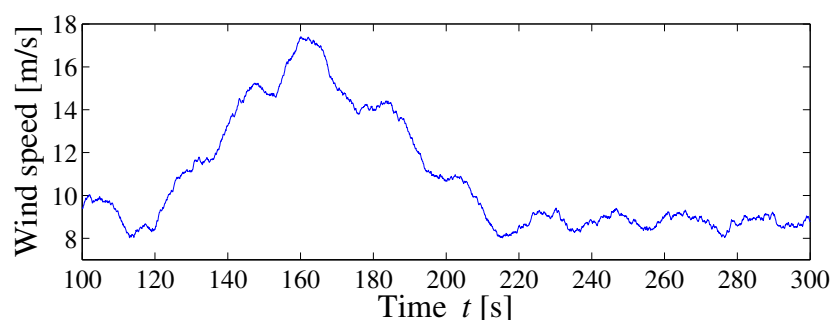
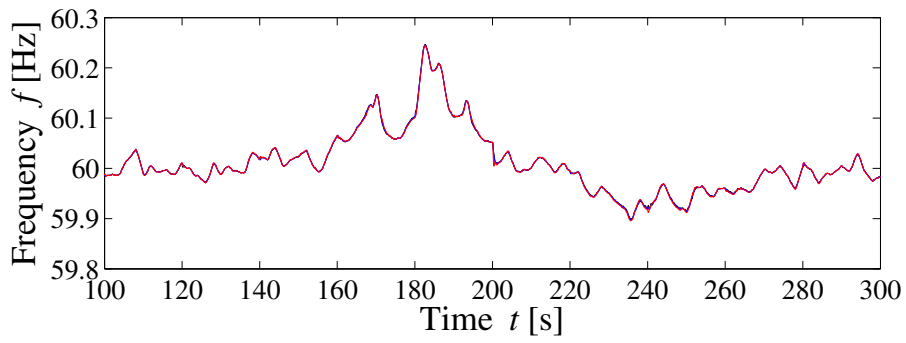
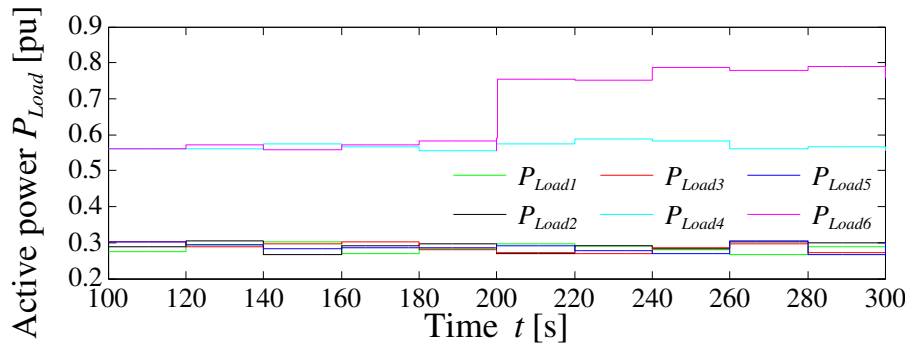


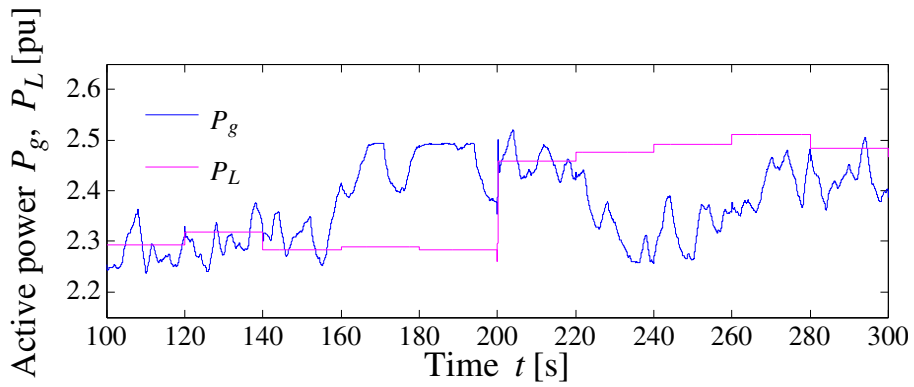
Figure 14. Wind speed.



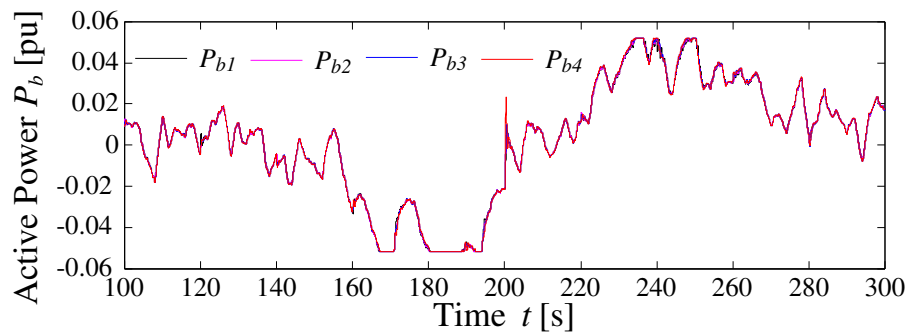
(a) frequency, f



(b) Consumption power of load of each bus, P_{Load}



(c) Active power of generator and load, P_g, P_L



(d) Active power of each battery, P_b

Figure 15. Cont.

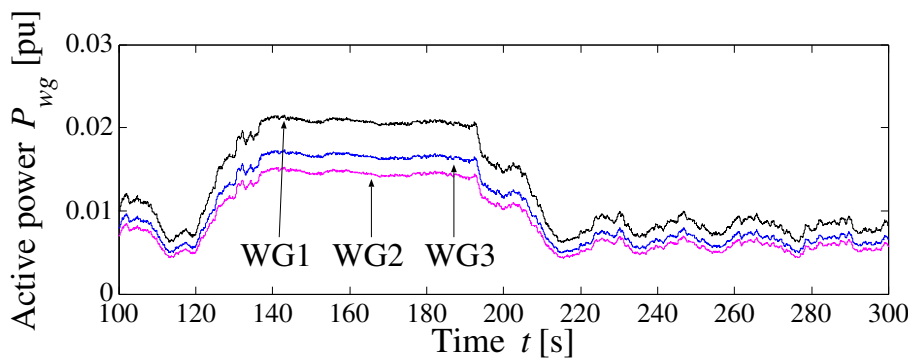
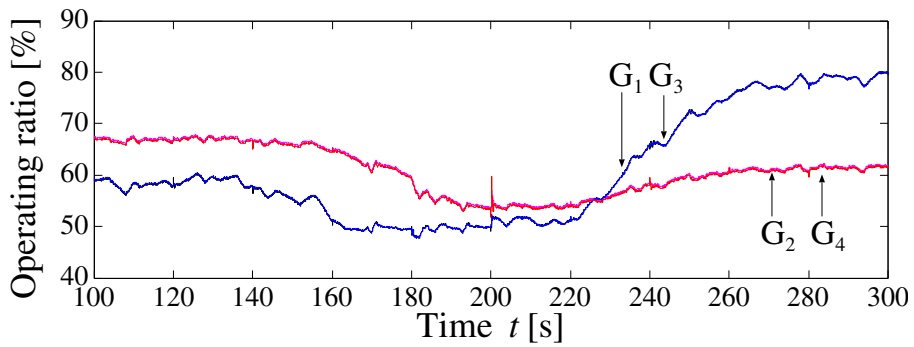
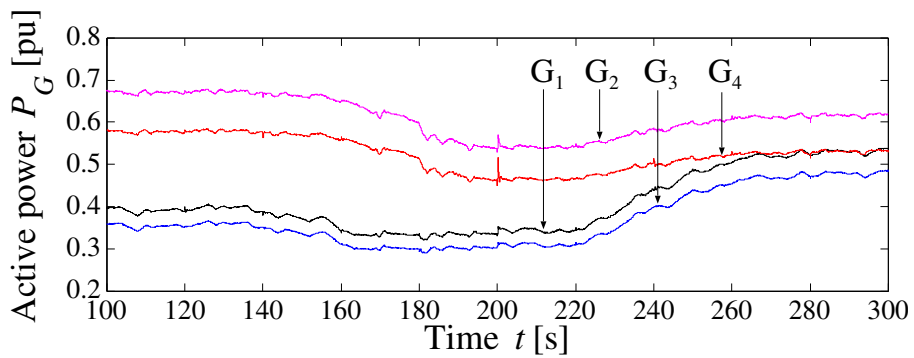
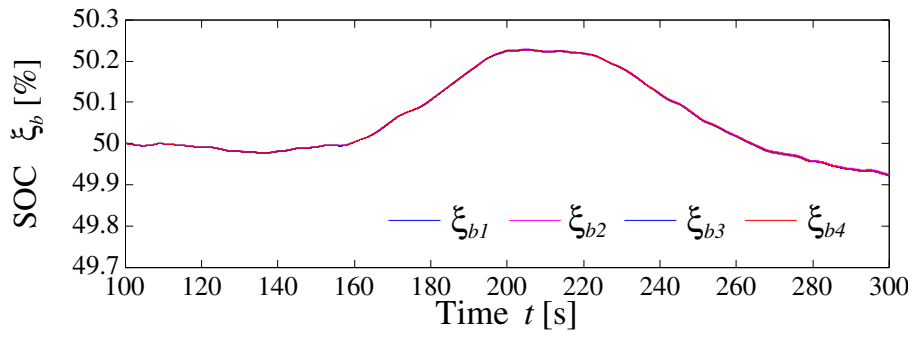
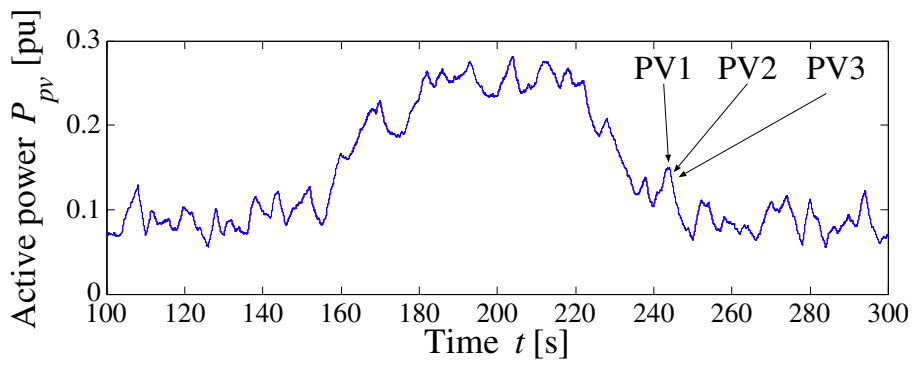
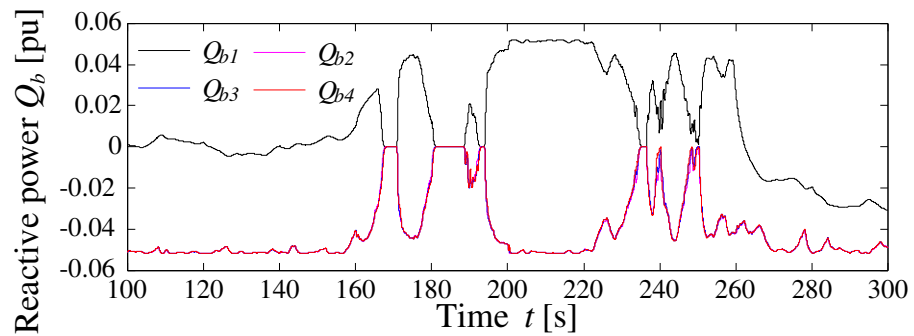


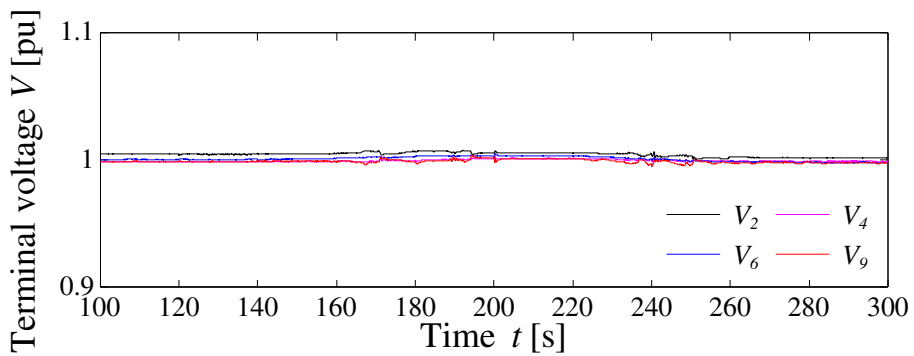
Figure 15. Cont.



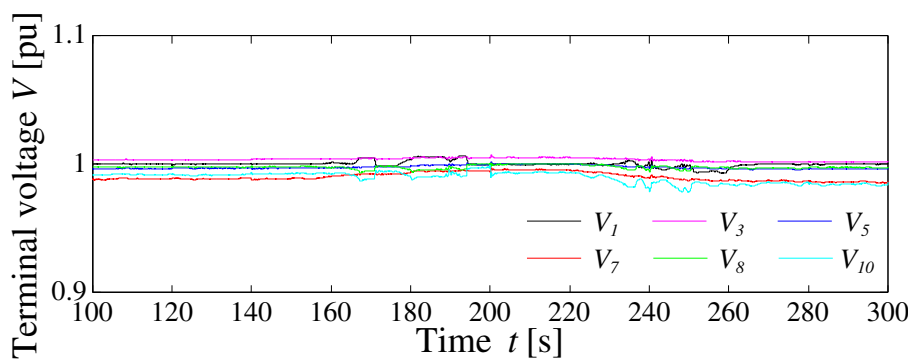
(i) Active power of photovoltaic generator, P_{pv}



(j) Reactive power of each battery, Q_{b1}

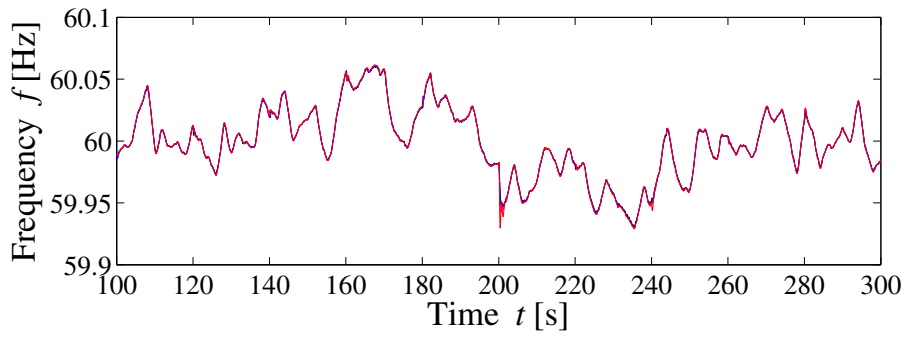


(k) Terminal voltage of generator side, V_2, V_4, V_6, V_9

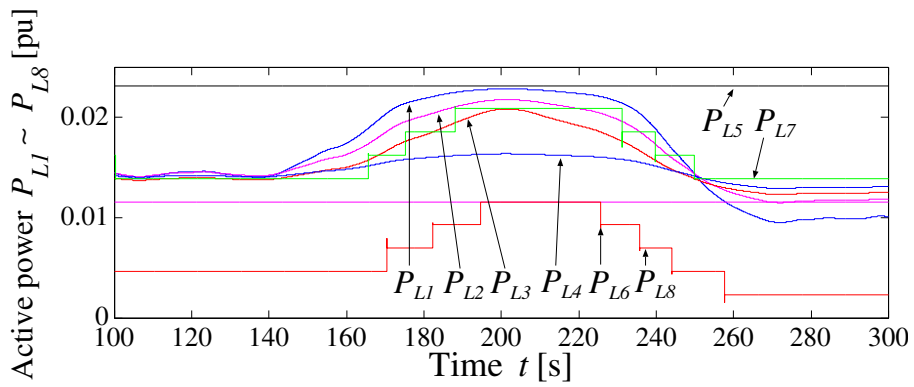


(l) Terminal voltage of load side, $V_1, V_3, V_5, V_7, V_8, V_{10}$

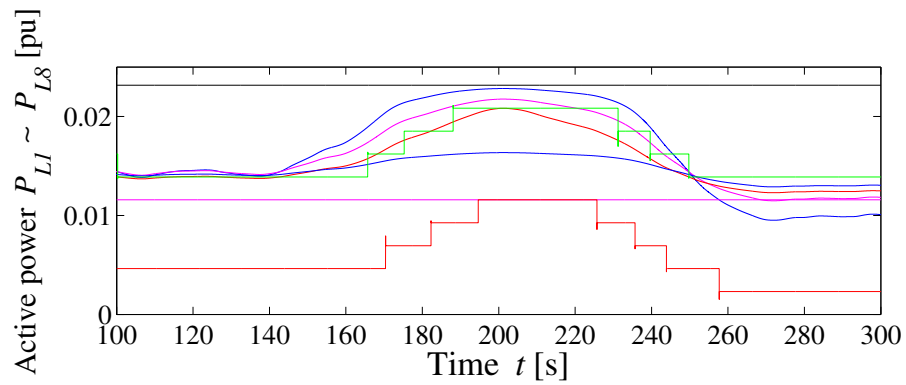
Figure 15. Simulation result of base case (with battery).



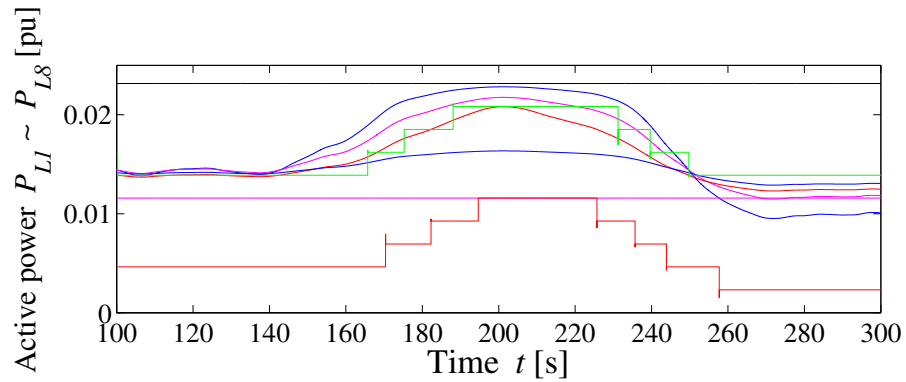
(a) Frequency, f



(b₁) Consumption power of each load for bus 1



(b₂) Consumption power of each load for bus 2



(b₃) Consumption power of each load for bus 3

Figure 16. Cont.

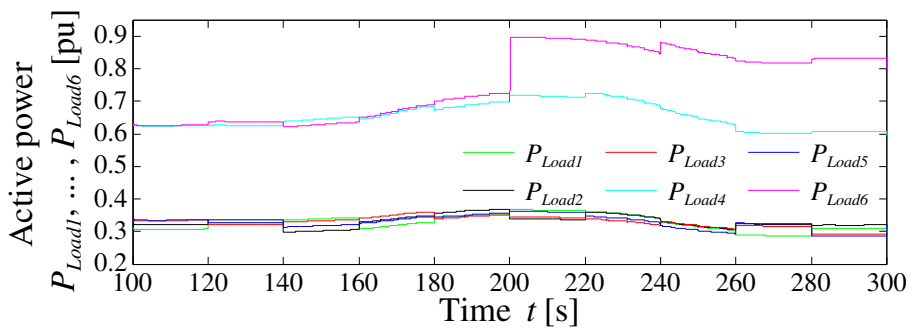
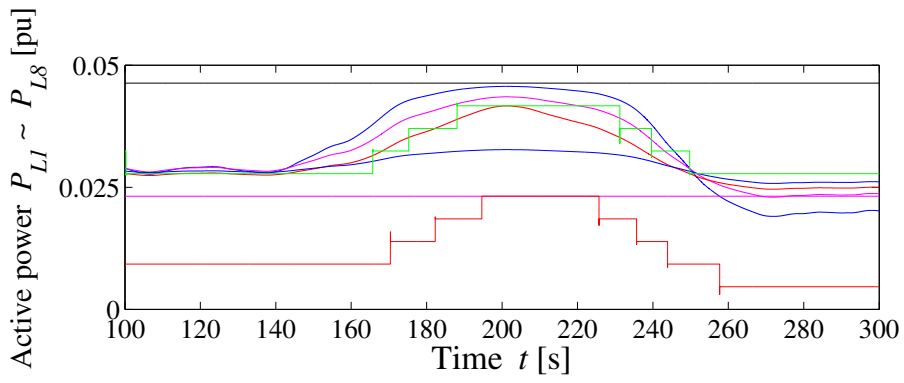
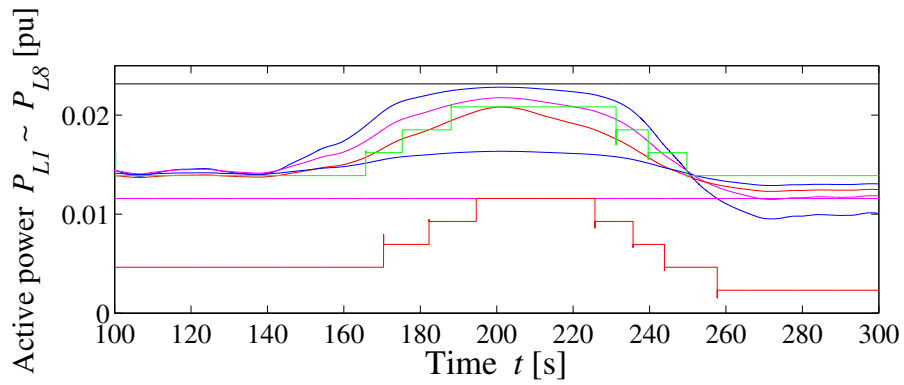
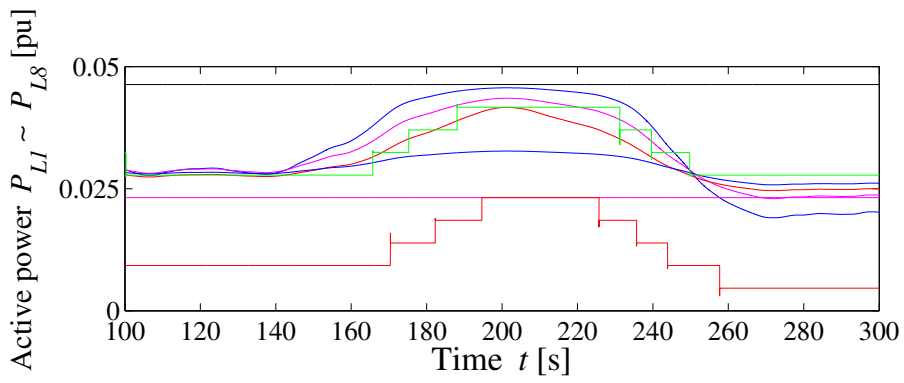
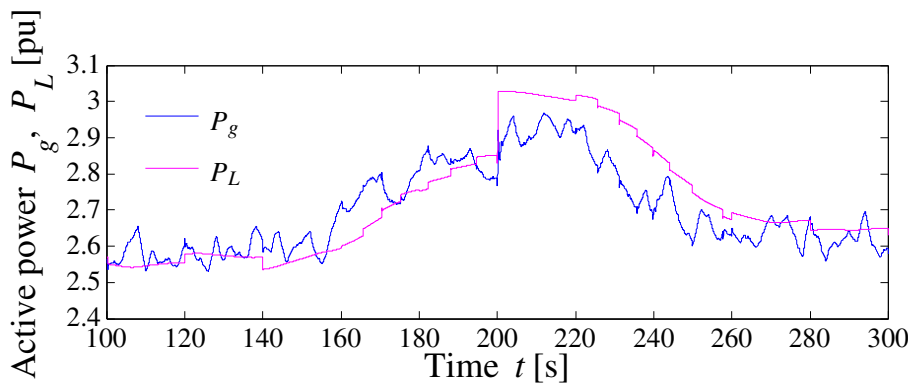
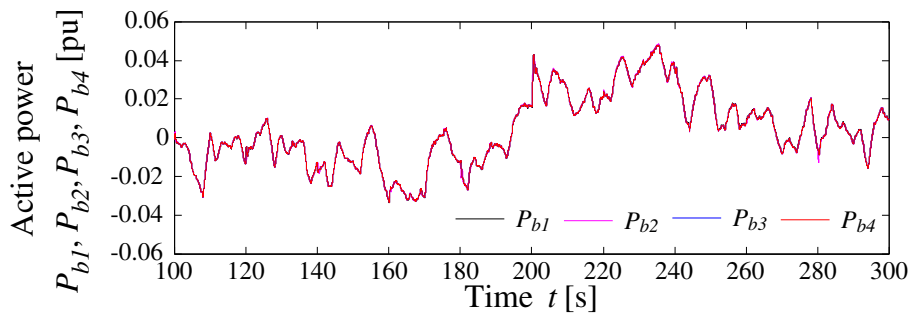


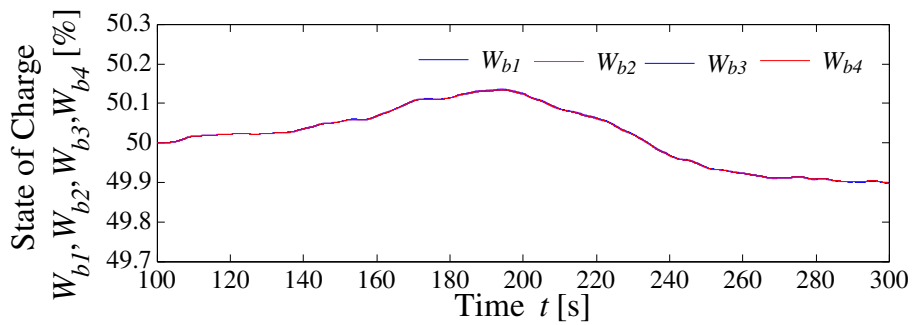
Figure 16. Cont.



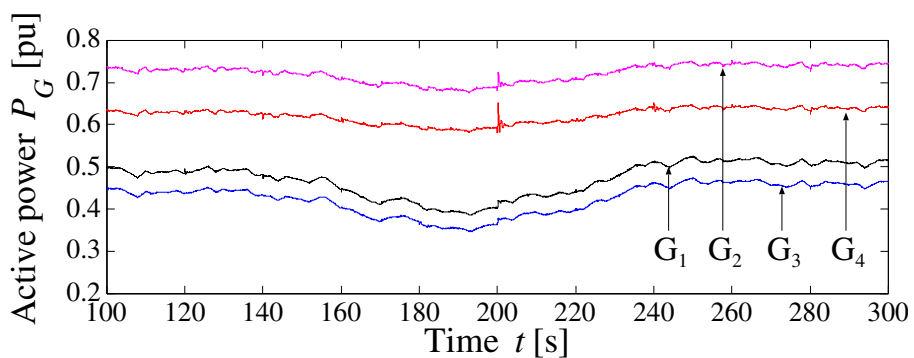
(d) Active power of generator and load, P_g, P_L



(e) Active power of each battery, P_b

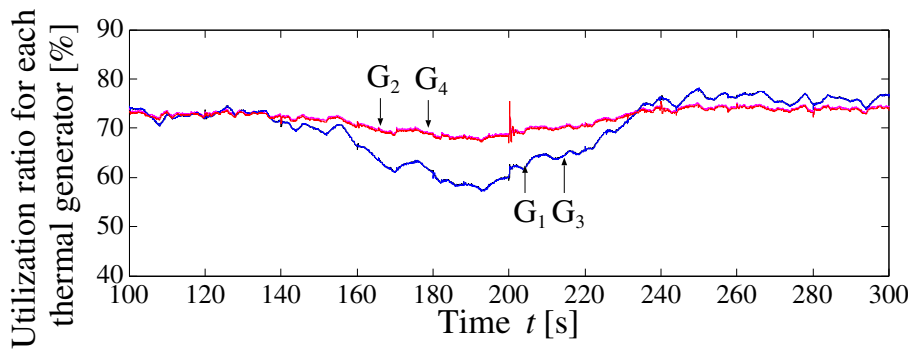


(f) State of charge of each battery, W_b

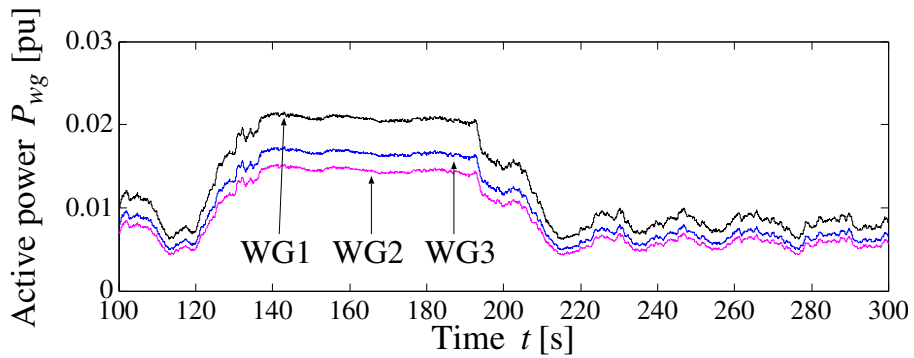


(g) Active power of thermal generator, P_G

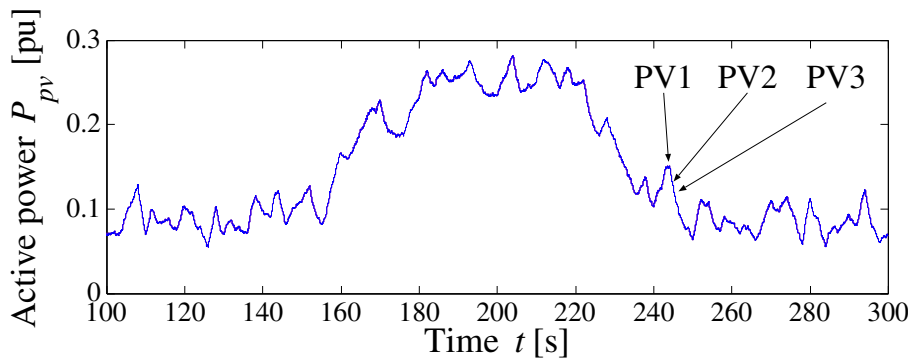
Figure 16. Cont.



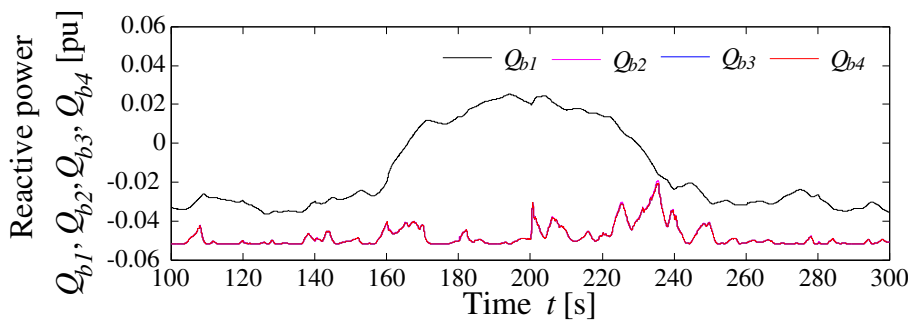
(h) Operation ratio for each thermal generator



(i) Active power of wind generator, P_{wg}

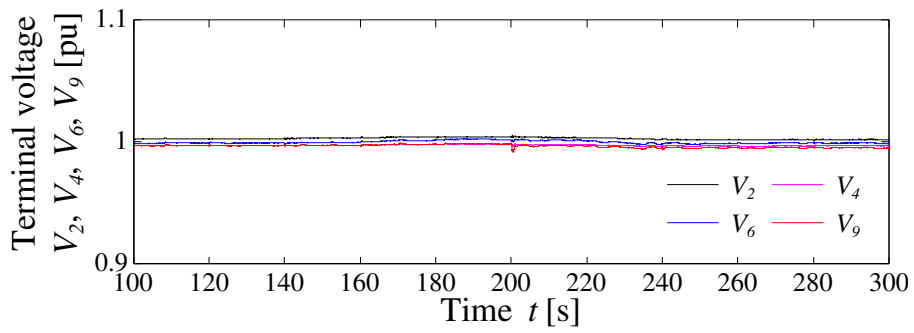


(j) Active power of photovoltaic generator, P_{pv}

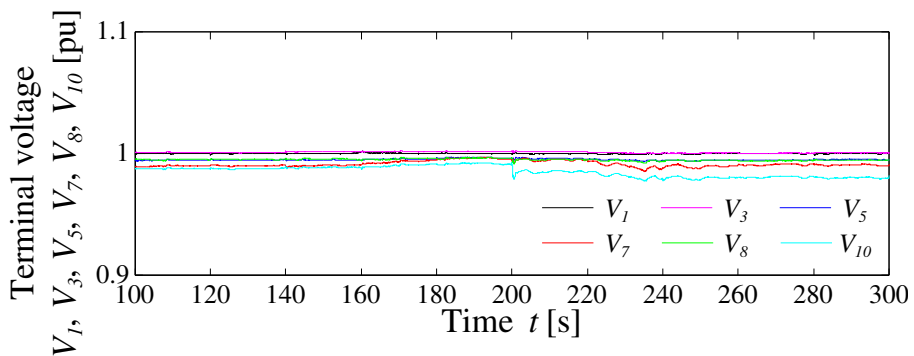


(k) Reactive power of each battery, Q_{b1} .

Figure 16. Cont.

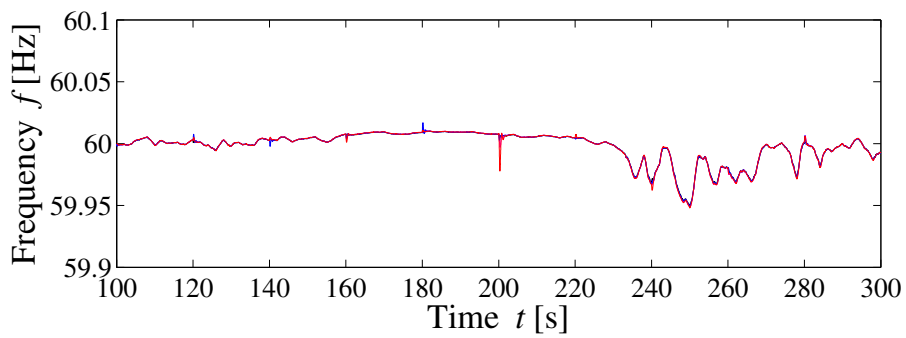


(l) Terminal voltage of generator side V_2, V_4, V_6, V_9 .

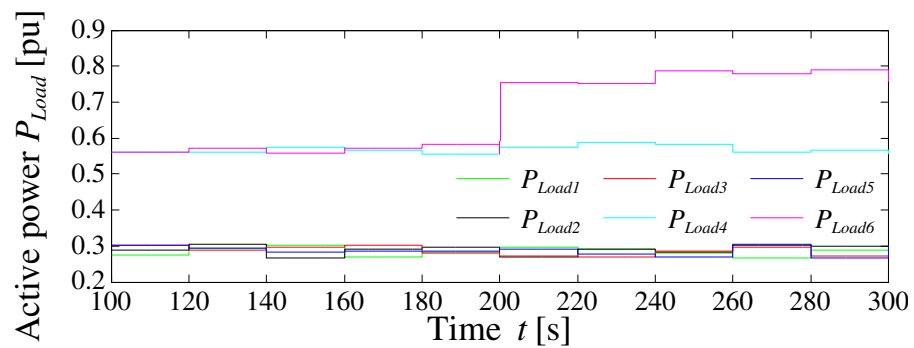


(m) Terminal voltage of load side $V_1, V_3, V_5, V_7, V_8, V_{10}$

Figure 16. Simulation result (with battery and demand response).

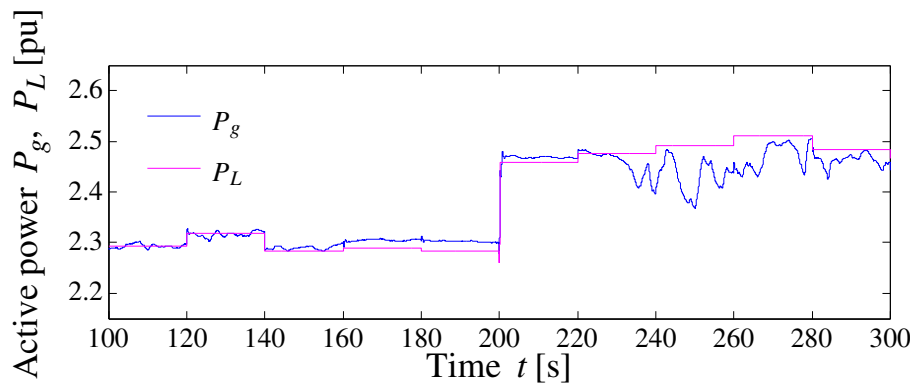


(a) Frequency, f

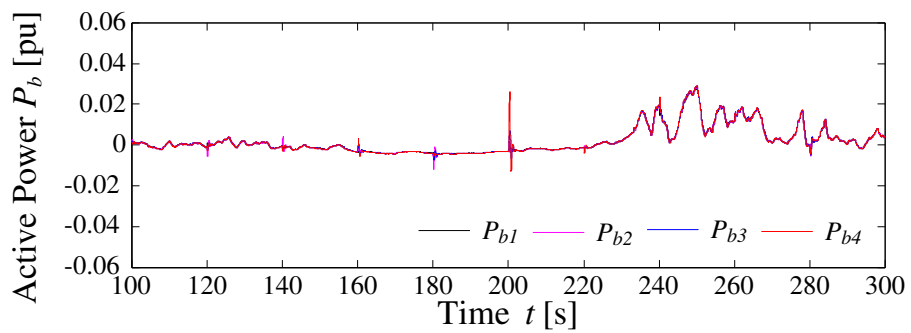


(b) Consumption power of load of each bus, P_{Load}

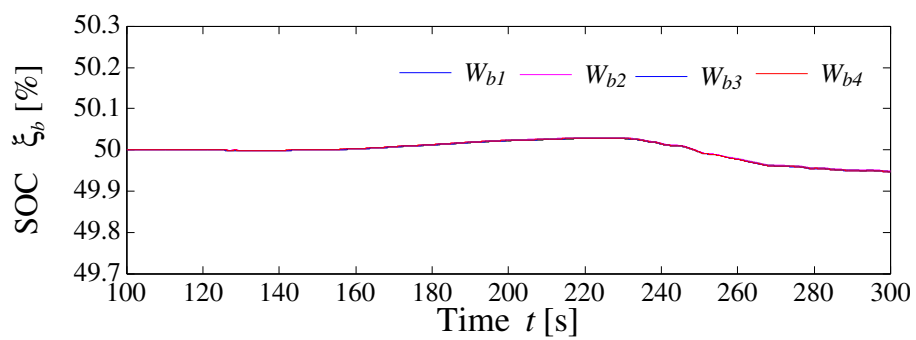
Figure 17. Cont.



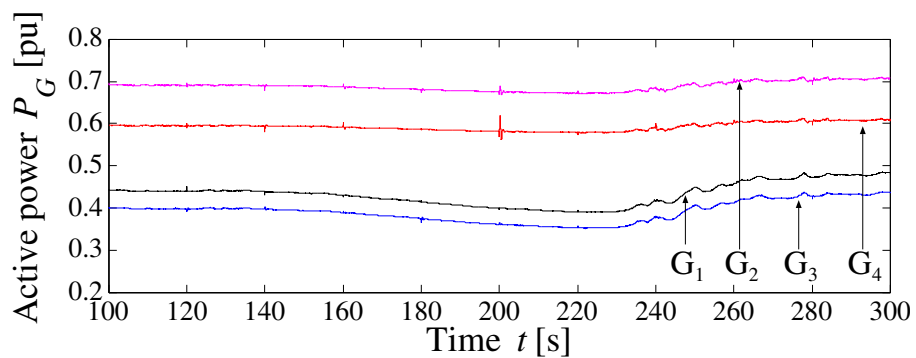
(c) Active power of generator and load, P_g, P_L



(d) Active power of each battery, P_b

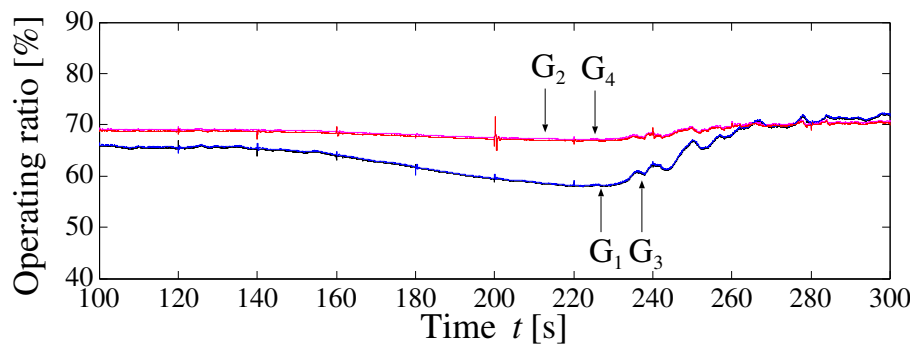


(e) State of charge of each battery, W_b

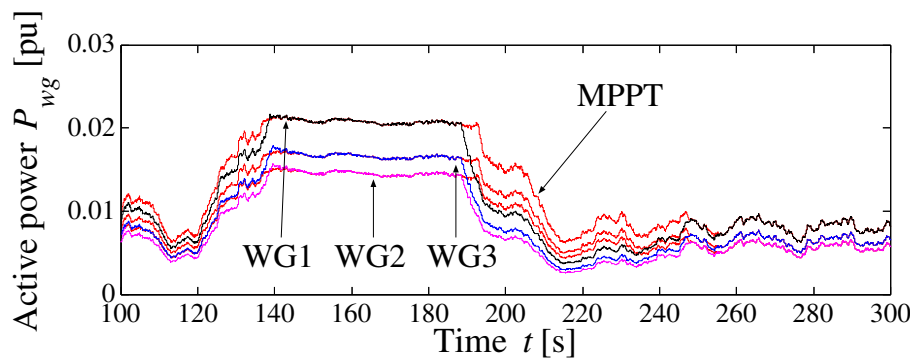


(f) Active power of thermal generator, P_G

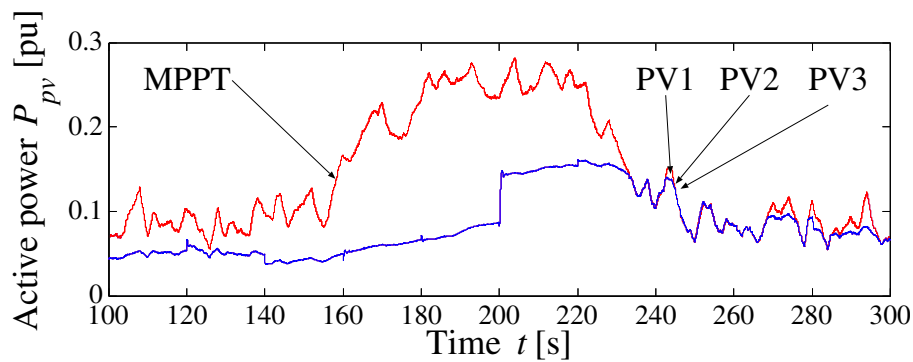
Figure 17. Cont.



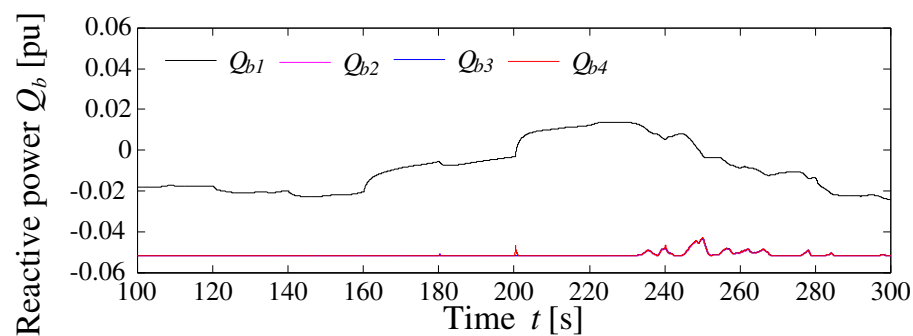
(g) Operation ratio for each thermal generator



(h) Active power of wind generator, P_{wg}

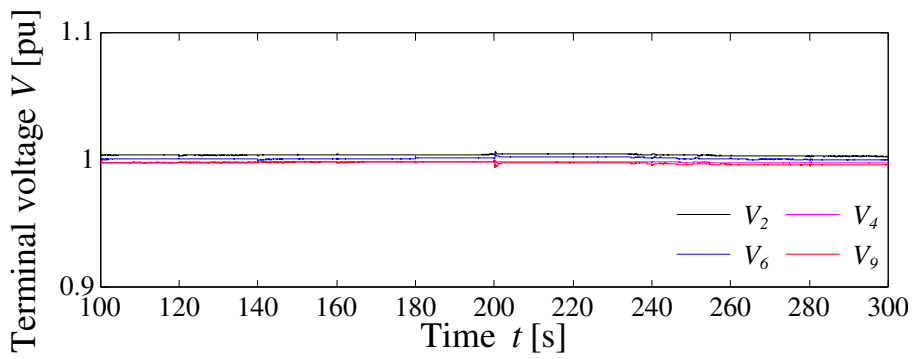


(i) Active power of photovoltaic generator, P_{pv}

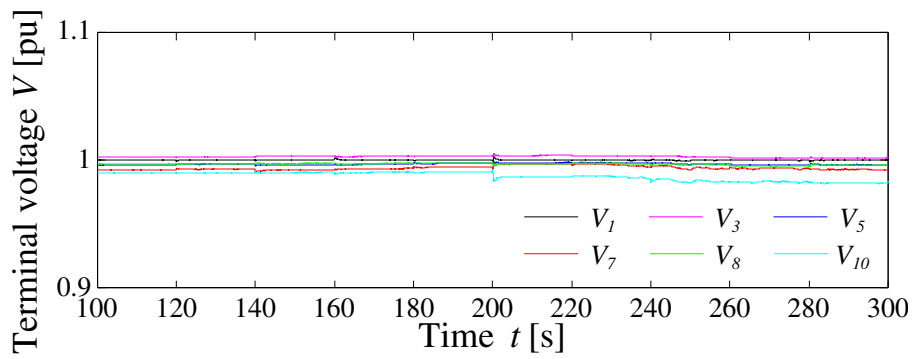


(j) Reactive power of each battery, Q_{b1} .

Figure 17. Cont.

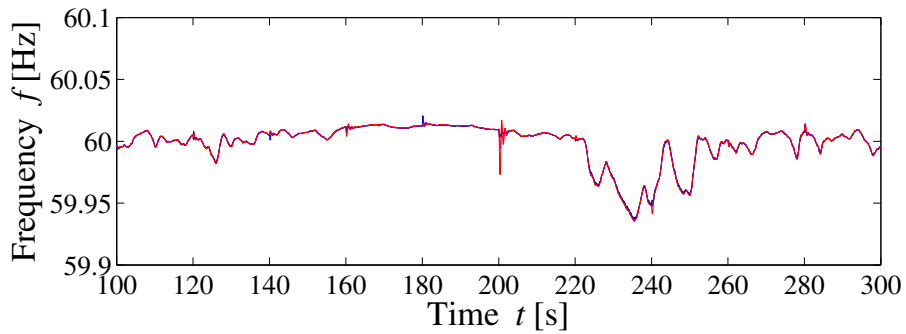


(k) Terminal voltage of generator side V_2, V_4, V_6, V_9

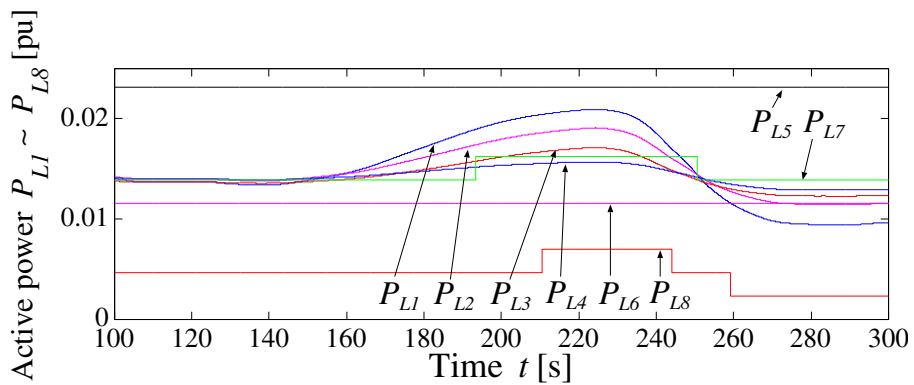


(l) Terminal voltage of load side $V_1, V_3, V_5, V_7, V_8, V_{10}$

Figure 17. Simulation result (with battery and supply power suppression of renewable energy sources).

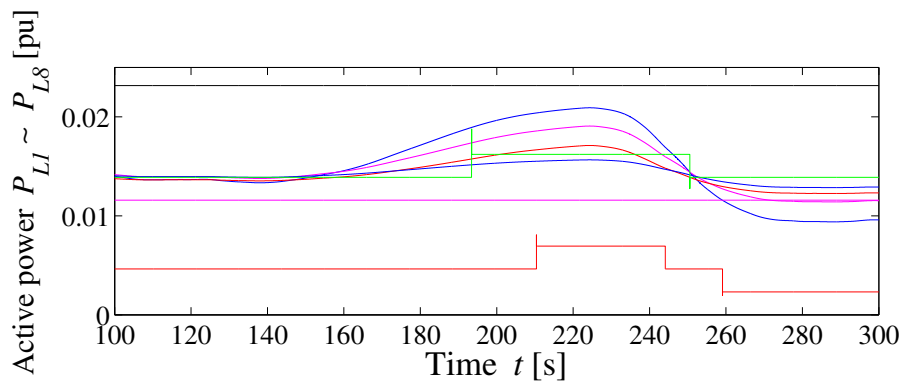


(a) Frequency, f

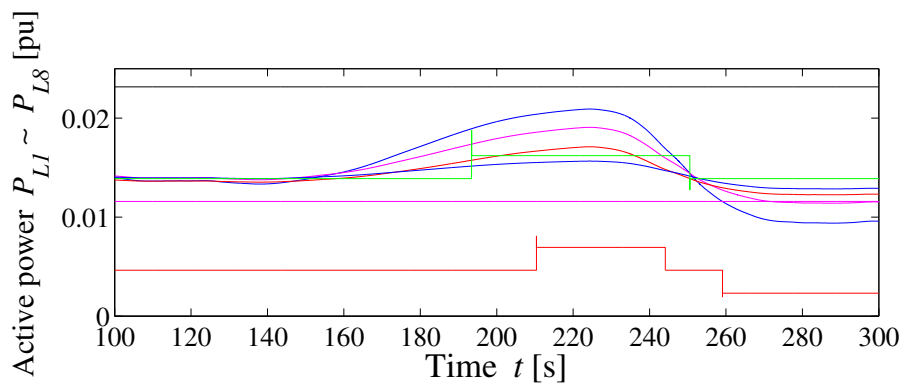


(b₁) Consumption power of each load for bus 1

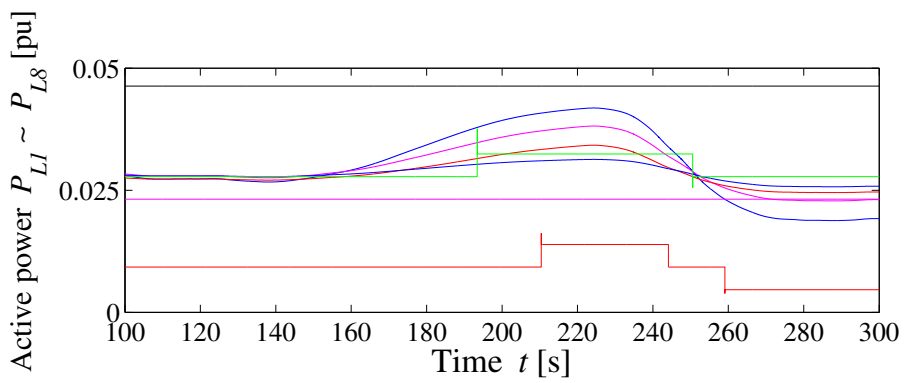
Figure 18. Cont.



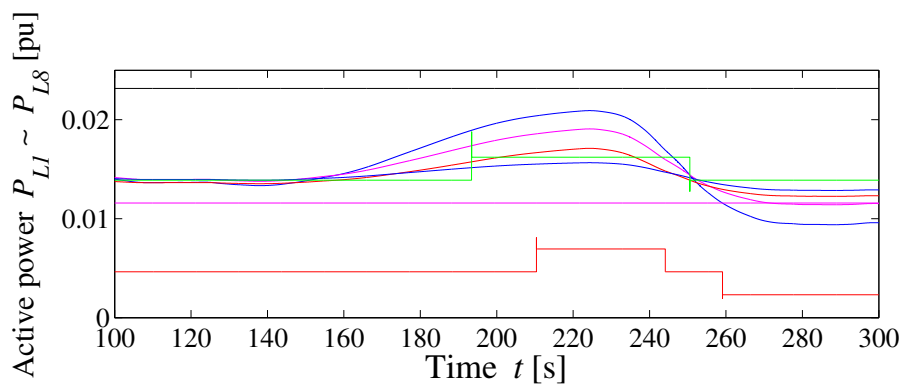
(b₂) Consumption power of each load for bus 2



(b₃) Consumption power of each load for bus 3

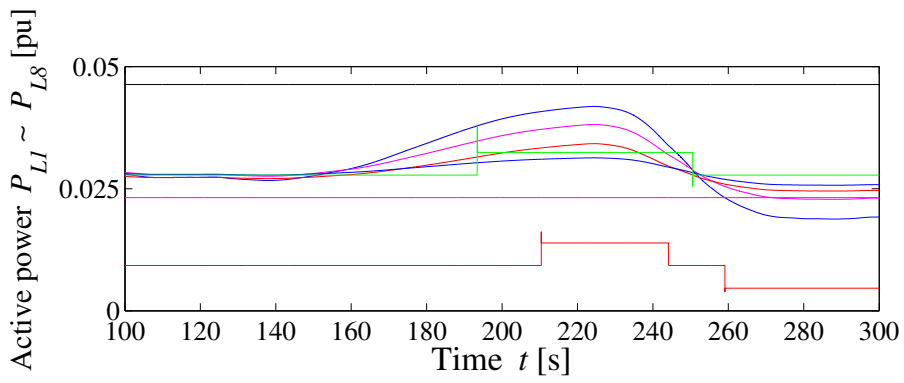


(b₄) Consumption power of each load for bus 4

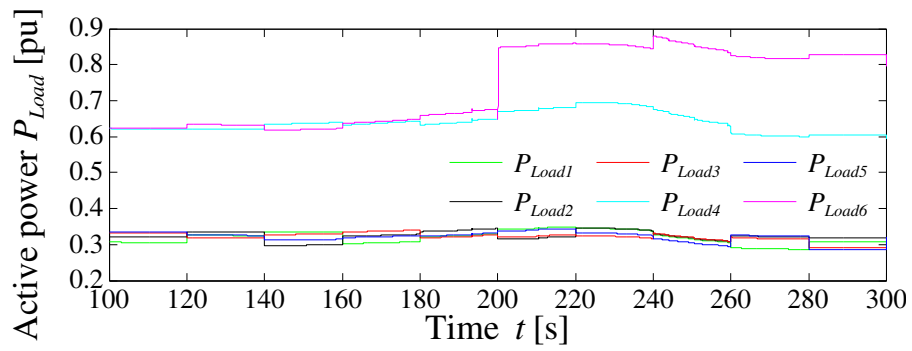


(b₅) Consumption power of each load for bus 5

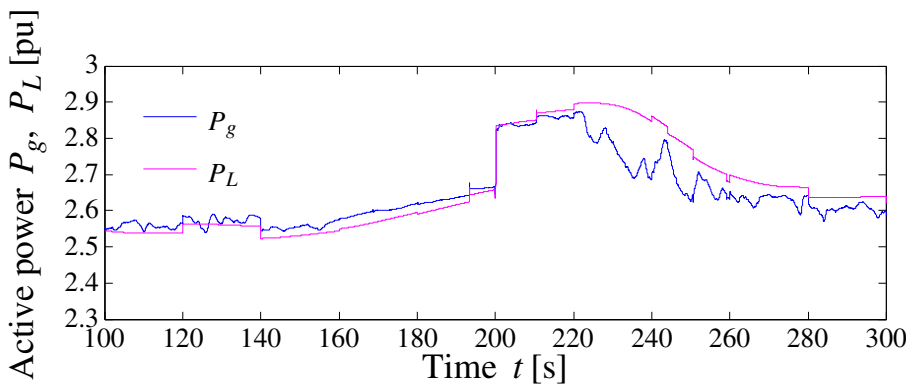
Figure 18. Cont.



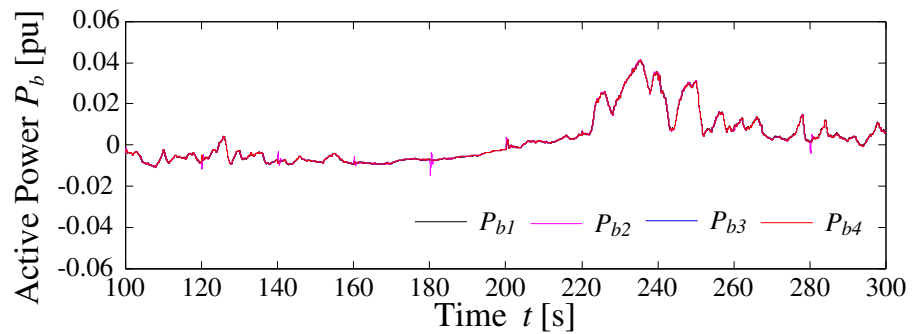
(b) Consumption power of each load for bus 6



(c) Consumption power of load of each bus, P_{Load}

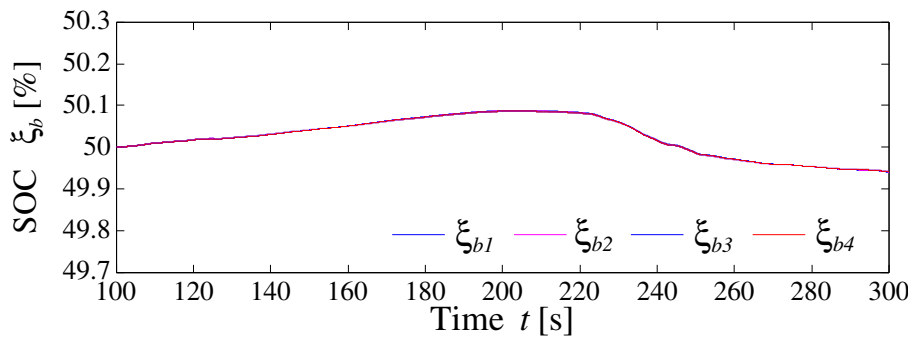


(d) Active power of generator and load, P_g, P_L

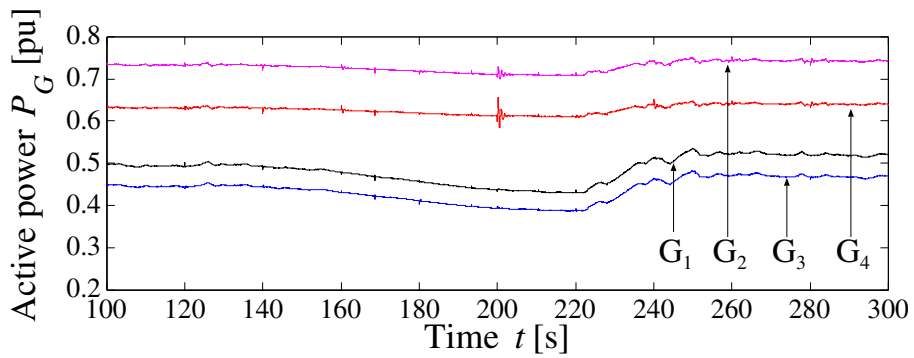


(e) Active power of each battery, P_b

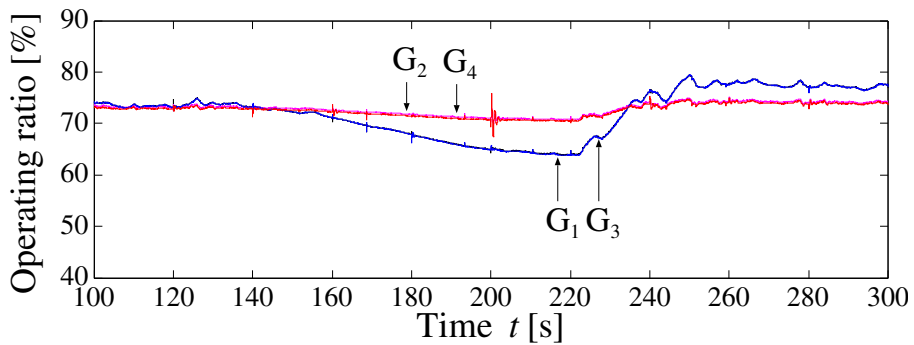
Figure 18. Cont.



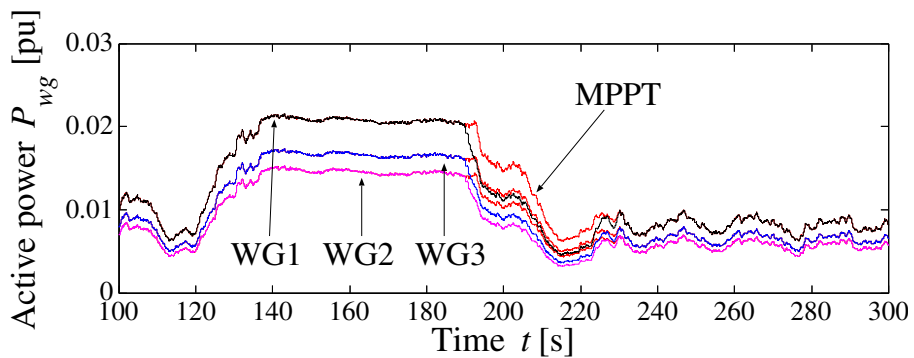
(f) State of charge of each battery, W_b



(g) Active power of thermal generator, P_G

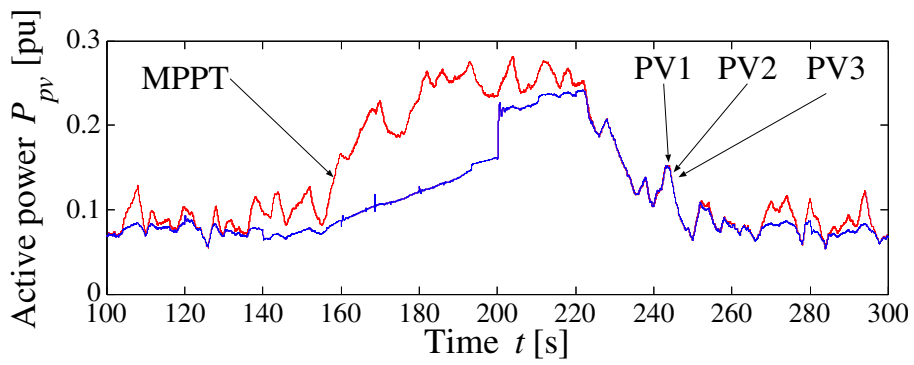


(h) Operation ratio for each thermal generator

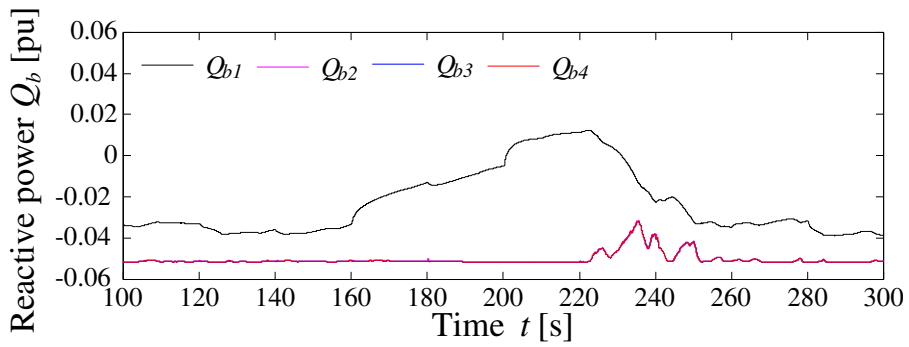


(i) Active power of wind generator, P_{wg}

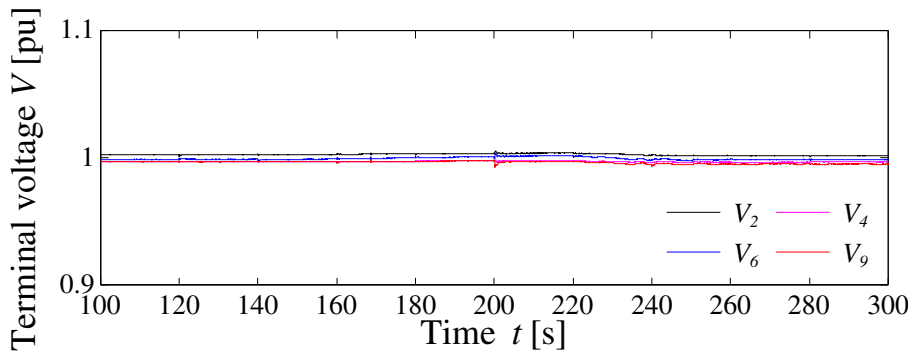
Figure 18. Cont.



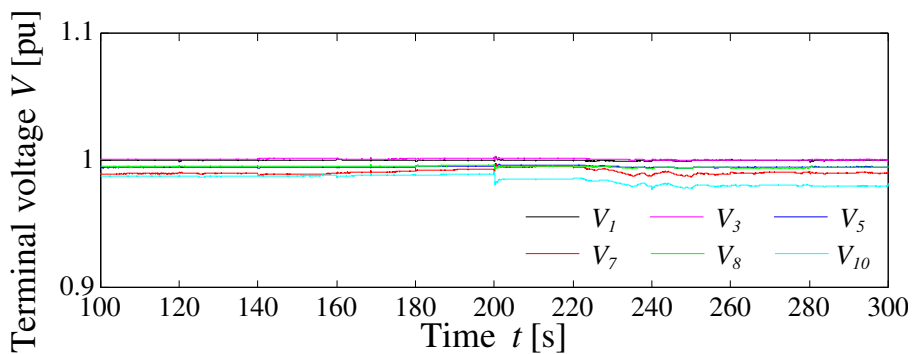
(j) Active power of photovoltaic, P_{pv} .



(k) Reactive power of each battery, Q_{b1}

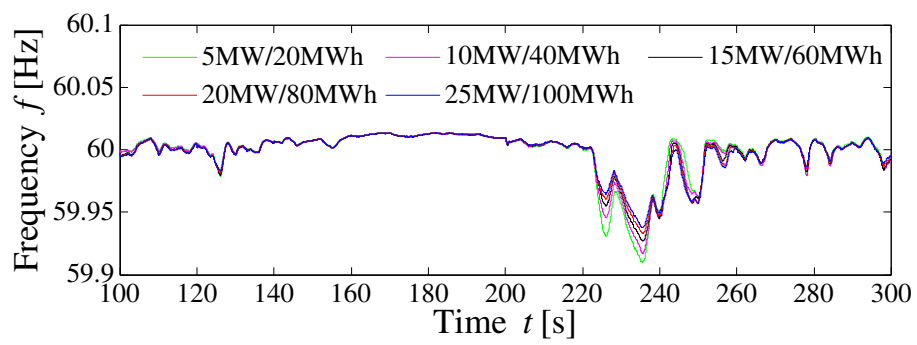


(l) Terminal voltage of generator side V_2, V_4, V_6, V_9

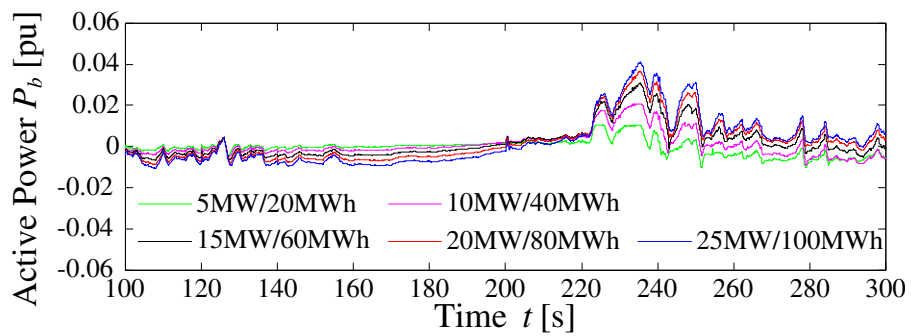


(m) Terminal voltage of load side $V_1, V_3, V_5, V_7, V_8, V_{10}$

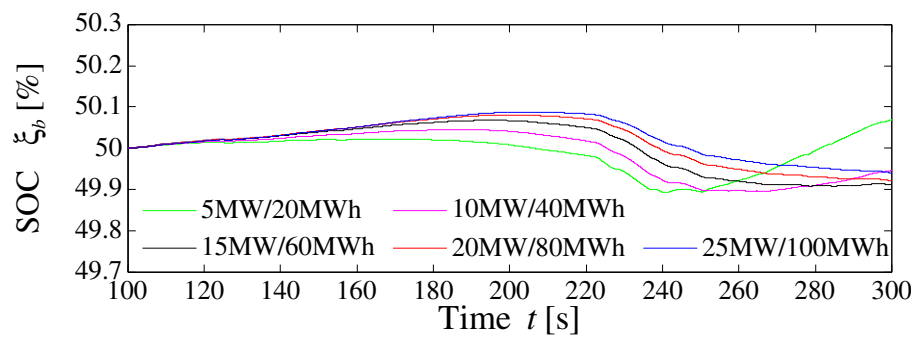
Figure 18. Simulation result (with battery, suppression of renewable energy sources, and demand response).



(a) Frequency, f

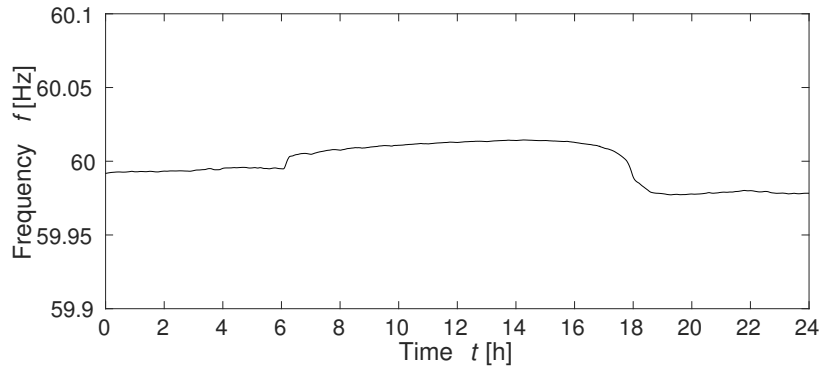


(b) Active power of battery 1, P_b

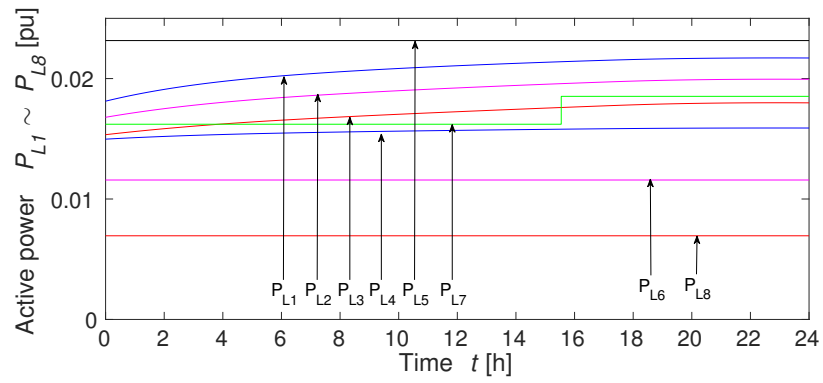


(c) State of charge of battery, W_b

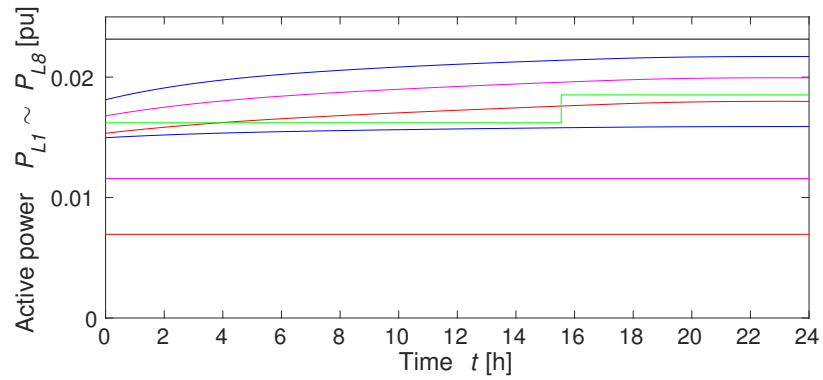
Figure 19. Simulation result for comparison of installed capacities of battery (with battery, supply power suppression of renewable energy source and demand response).



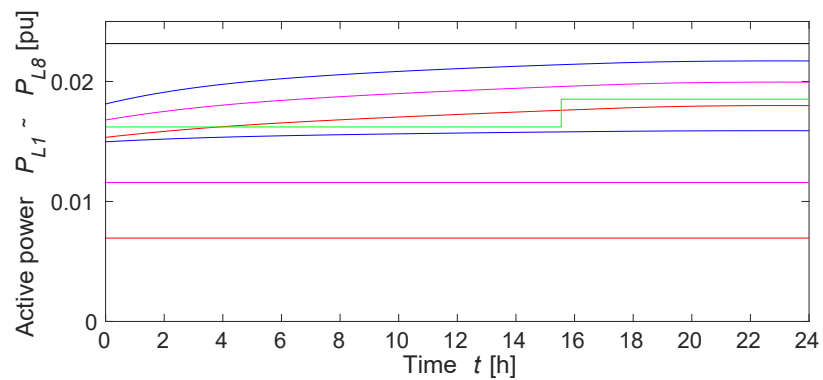
(a) Frequency, f



(b₁) Consumption power of each load for bus 1

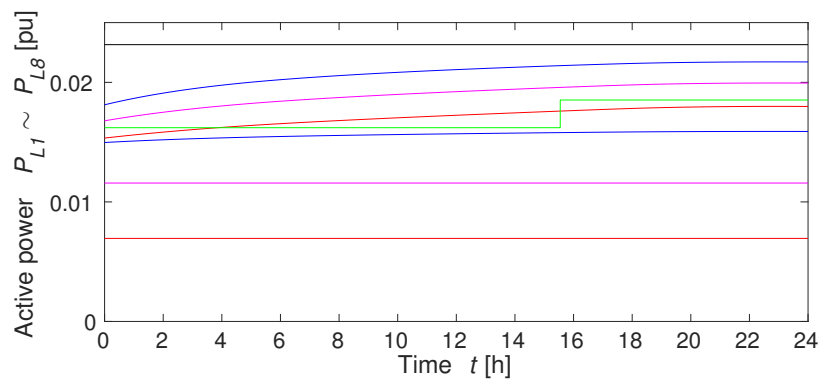


(b₂) Consumption power of each load for bus 2

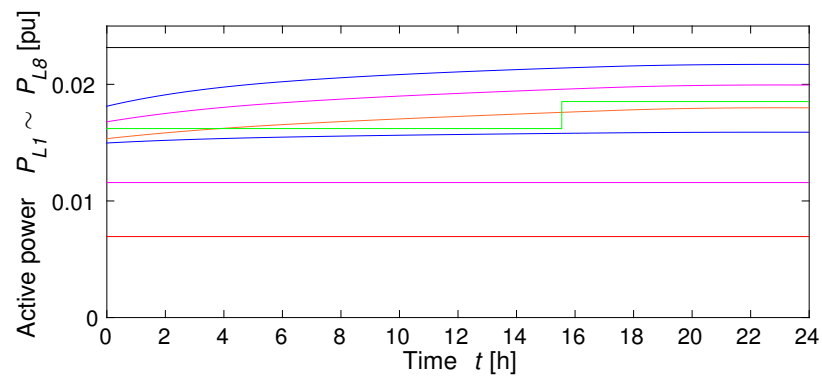


(b₃) Consumption power of each load for bus 3

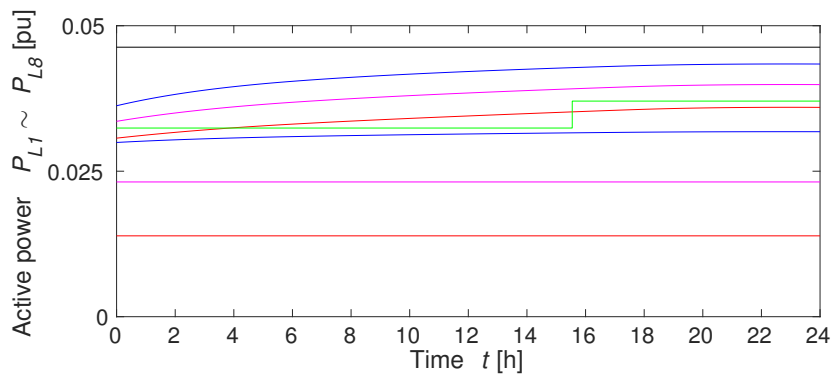
Figure 20. Cont.



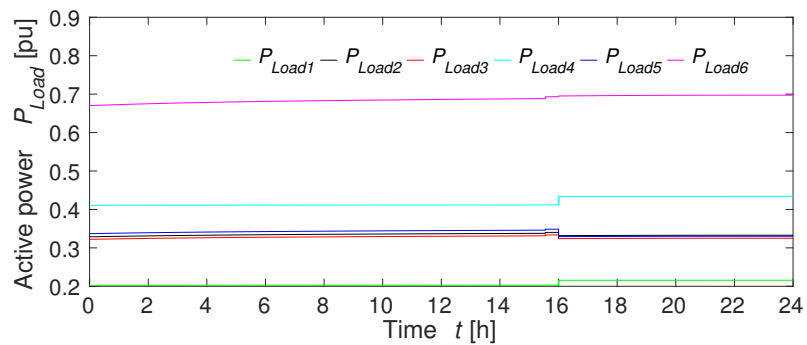
(b₄) Consumption power of each load for bus 4



(b₅) Consumption power of each load for bus 5

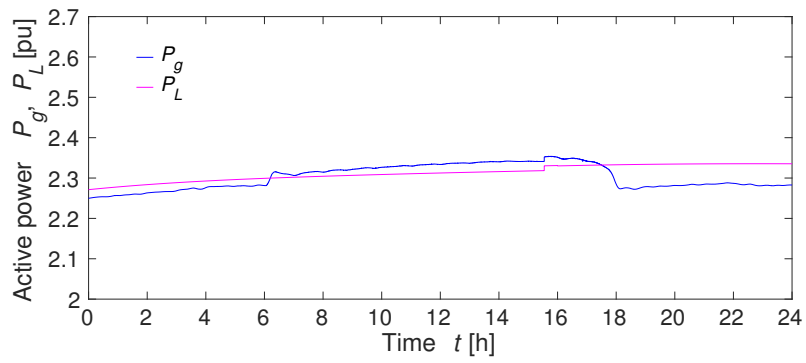


(b₆) Consumption power of each load for bus 6

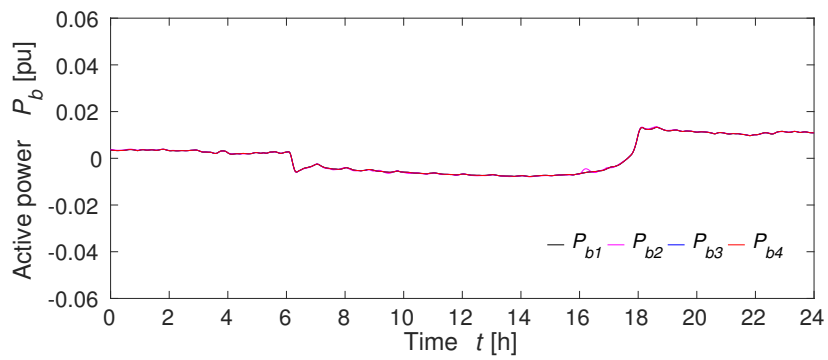


(c) Consumption power of load of each bus, P_{Load}

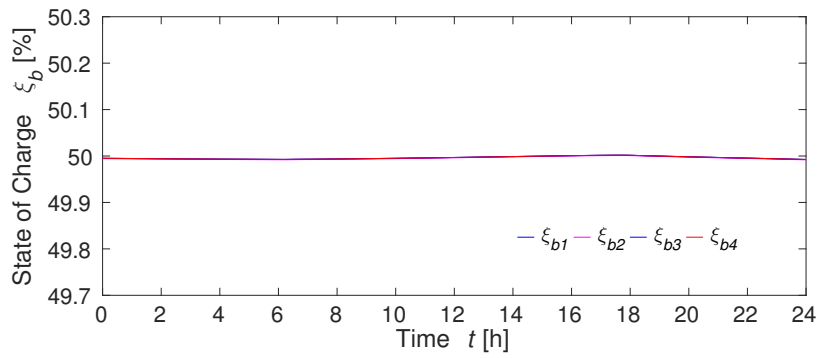
Figure 20. Cont.



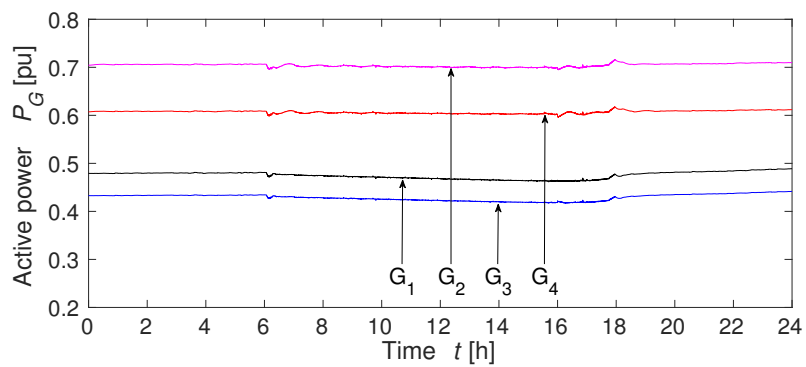
(d) Active power of generator and load, P_g, P_L



(e) Active power of each battery, P_b

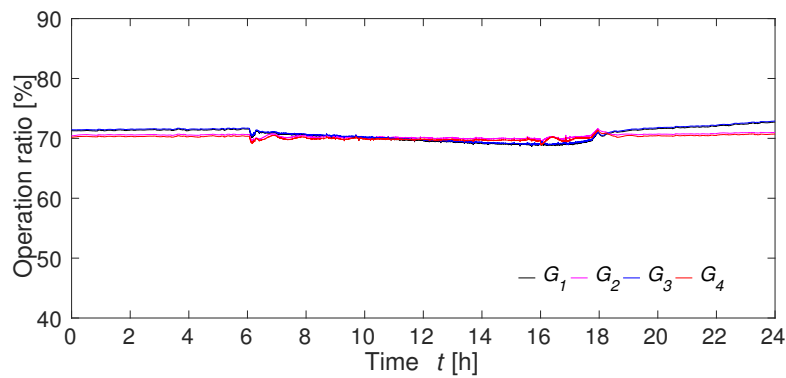


(f) State of charge of each battery, W_b

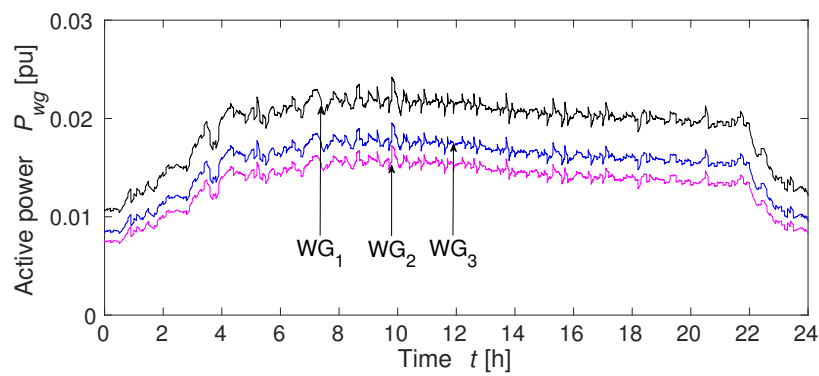


(g) Active power of thermal generator, P_G

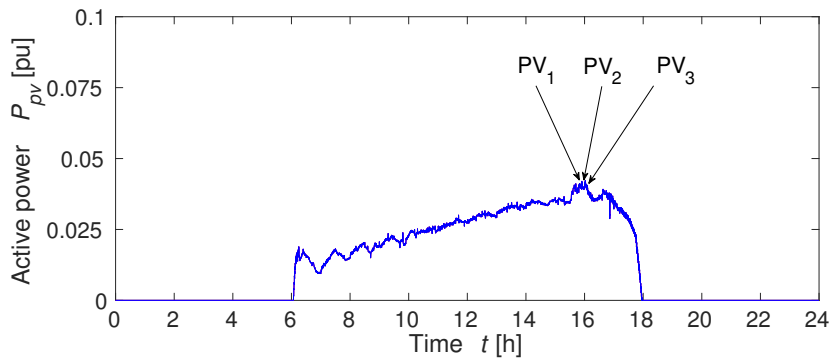
Figure 20. Cont.



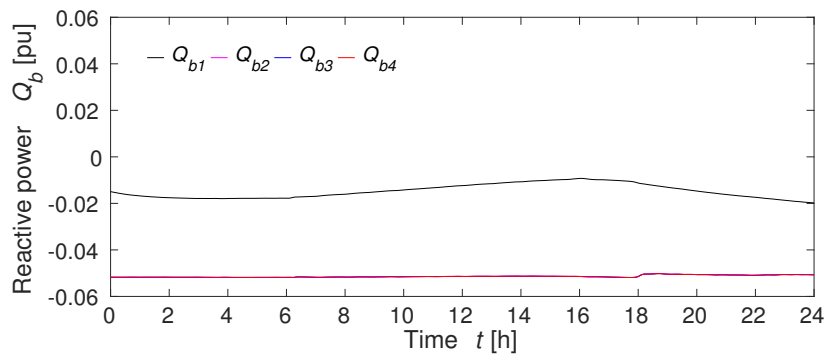
(h) Operation ratio for each thermal generator



(i) Active power of wind generator, P_{wg}

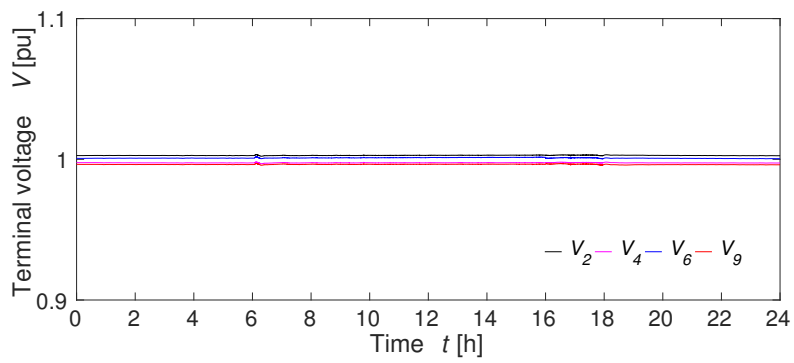


(j) Active power of photovoltaic, P_{pv} .

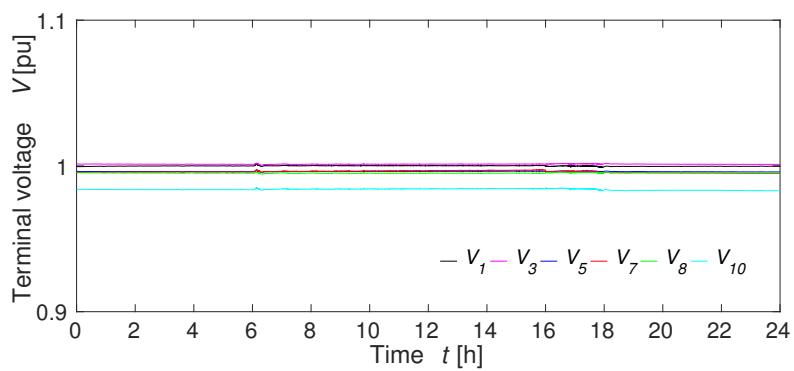


(k) Reactive power of each battery, Q_{b1}

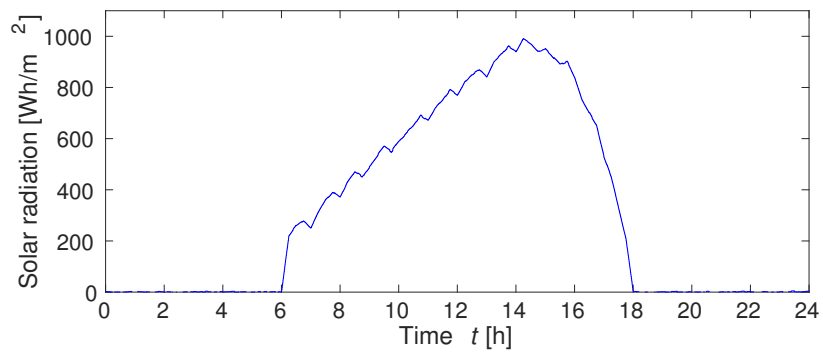
Figure 20. Cont.



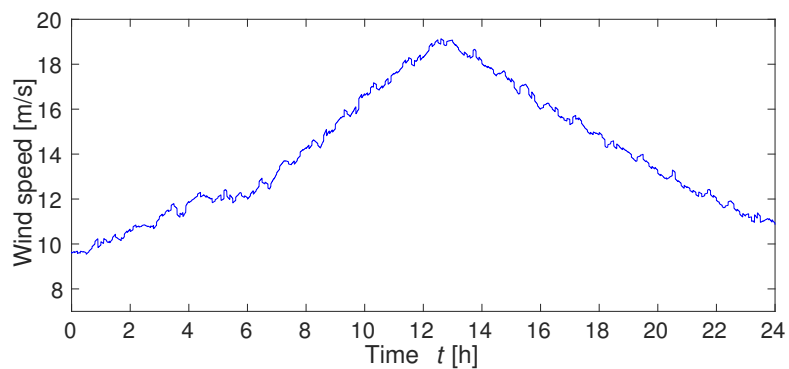
(l) Terminal voltage of generator side V_2, V_4, V_6, V_9



(m) Terminal voltage of load side $V_1, V_3, V_5, V_7, V_8, V_{10}$



(n) Solar radiation for 24 h case



(o) Wind speed for 24 h case

Figure 20. Simulation result for 24 h case (with battery, suppression of renewable energy sources and demand response).

7. Examination

7.1. Examination of the Simulation Result of Load Frequency Control Using Storage Battery and Demand-Response and Comparison to the Base Case Study

First, by comparing Figure 15a and Figure 16a, it can be seen that the fluctuation of load frequency had been controlled. This is because the stability of supply-demand balance had been improved thanks to consumption power flexibility of the controllable loads in Figure 16b,c. Figure 16d shows the generated power of each generator and consumption. As can be noticed from here, the difference between generated power and consumption power has to be small by fluctuating consumption power. For Figure 16e, compared to Figure 15d, by using demand response, the load is controllable even the inverter capacity of battery did not reach the maximum value. Also, we can know by comparing Figure 16g,h and Figure 15f,g that the thermal generator can work without reaching 50% of the output lower limit value. From this, it is possible to introduce further renewable energy power because of creating few margins by using demand response. From Figure 16l,m it can be confirmed that each bus voltage was in the allowable value. The next section will show the simulation results of output control using storage battery with renewable energy generation.

7.2. Examination of the Simulation Result of Load Frequency Control Using Storage Battery and Renewable Energy Generation Output Control Method and Comparison to the Base Case Study

In this part, the simulation results of introducing storage battery shown in Figure 15, introducing storage battery and demand response method shown in Figure 16, introducing storage battery and renewable energy generation output control shown in Figure 17, would be compared and examined. First, compare Figures 15a, 16a and 17a, the fluctuation can be minimized by using output control of renewable energy generator. By Figure 16a, it has reduced the frequency fluctuation by using a rapid demand response method. Also, a frequency fluctuation maximum at 0.05 Hz occurs at $t = 240$ s. As Figure 15c and Figure 17c show, when output control of renewable energy generation is performed, the generated power and supplied power were almost equal, stability was greatly improved than compensation only by the storage battery. As shown in Figure 15d, when compensation is held only with battery, the inverter capacity can reach maximum value sometimes. In Figure 17d, storage battery compensated for the difference of demand-supply balance by demand response with low-frequency operation characteristics. However, when renewable energy output control is performed, inverter capacity of the battery will not reach maximum value anymore and renewable energy will only compensate steep output fluctuation. As a result, as shown in Figure 17e, the SOC fluctuation of each battery had been small. In addition, because of the weather condition had been worse at $t = 240$ s, so that maximum output of renewable energy generation decreased, which is the reason that the output of storage battery increased. Therefore, until thermal power generator adjusts output, storage battery would supply active power. In Figure 15f,g, thermal power generators G1 and G3 have high response speeds at the lowest output and had no margin. In Figure 17f,g, it can be confirmed that a reduction rate of 10% remains. This makes it possible to avoid oversupply by power consumption reduction and the further increase of generated power of renewable energy generation. From Figure 17h,i, it can be seen that PV and WG power generation have been controlled. Also, the effect of output control of PV is better than output control of WG because there had a servo system delay in WG pitch angle control system. Due to this delay, original output power suppressed by WG changed to be suppressed by PV. By output control of renewable energy generation, it is possible to increase renewable energy supply power by changing the operating point momentarily when load demand suddenly increased. As shown in Figure 17k,l, the voltage of each bus is within the permissible values. From above, it became possible to stabilize the system frequency by using output power control of renewable energy generation. However, output control of renewable energy generation is not desirable by the effective use of energy. Therefore, in the next section, we will discuss system frequency control that combines output control of renewable energy generation and demand response.

7.3. Examination of the Simulation Result of Load Frequency Control Using Storage Battery, Renewable Energy Generation, Demand-Response and Comparison to the Base Case Study

By compensation of storage battery output control and renewable energy generation, here we will verify the effectiveness of the proposed scheme by adding demand response. Compare and examine Figures 17 and 18. First, from Figures 17a and 18a, we can find that frequency fluctuation can be suppressed in both cases. The maximum allowable frequency fluctuation range is 0.05 Hz as shown in Figure 17a and in Figure 18a it varies up to 0.06 Hz. Also the required time for system frequency to converge to 60 Hz in case of using demand response is shorter than not using. From Figure 18c due to compensating step disturbance, to reduce load power consumption. The power consumption of each load in Figure 18b varies according to electricity price. Load group connected to each bus changes as shown in Figure 18c. Stepwise change of P_{load6} shows the assumed disturbance. Figure 17d,e and Figure 18e,f perform almost the same operation. In Figure 18e, the output is slightly larger than the output in Figure 17d, and this is due to the first order lag of 10 s which is adopted in demand response pricing. Even difference of supply-demand balance became large, demand steeply increases, load demand also increased. However, in the case of using demand response and because of changing power consumption, frequency fluctuation can be quickly suppressed. So that battery only work as high-speed output fluctuation according to renewable energy generation. As a result, power consumption can be changed by introducing demand response and it is possible to adjust the difference of supply-demand balance not only from power supply side but also from the consumer side. So reduction of storage battery capacity will be possible. From Figure 18g,h, with adjusting high-speed response thermal output, maximization of renewable energy generation output and the supply-demand balance is hoped to be maintained. For renewable energy generation, and by comparing. Figure 17h,i and Figure 18i,j, output in Figure 18i,j is larger. This is because the fact that power consumption can be increased by demand response. In Figure 18l,m, the voltage of each bus is within 1 ± 0.059 pu, so it is in the allowable range. As above, with the output control of storage battery and renewable energy generation and by adding demand response, system frequency stabilization and renewable energy generation maximum had been achieved. Moreover, it is also possible to discuss the storage battery capacity reduction demand response.

7.4. Discussion about Capacity Reduction of Storage Battery

From the simulation results in the previous subsection, it inferred that storage capacity could be reduced by using demand response. In this subsection, we will discuss the reduction of storage battery capacity. Simulation conditions are the same as the previous subsection, and the case of system output control by using storage battery, renewable energy generator and demand response is assumed. Inverter capacity and storage capacity are as a parameter of the storage battery. In the previous subsection, it was assumed that inverter capacity/storage capacity of one battery is 25 MW/100 MWh. In this subsection, we conduct a simulation of 5 MW/20 MWh, 10 MW/40 MWh, 15 MW/60 MWh, 20 MW/80 MWh and examine the possibility of reducing the capacity of the storage battery. Figure 19 shows simulation results for comparing installed capacity of each battery. Figure 19a shows frequency, Figure 19b shows the output of battery 1, Figure 19c shows the state of charge (SOC) of battery 1. From Figure 19a,b, system frequency can be maintained within the allowed range even with reducing the capacity of the battery. As shown in Figure 19c, when the installed capacity of the battery was reduced, the fluctuation of SOC became larger. However, we can confirm that it is possible to reduce the capacity of the battery using the proposed method with keeping the frequency deviation in the permissible limit.

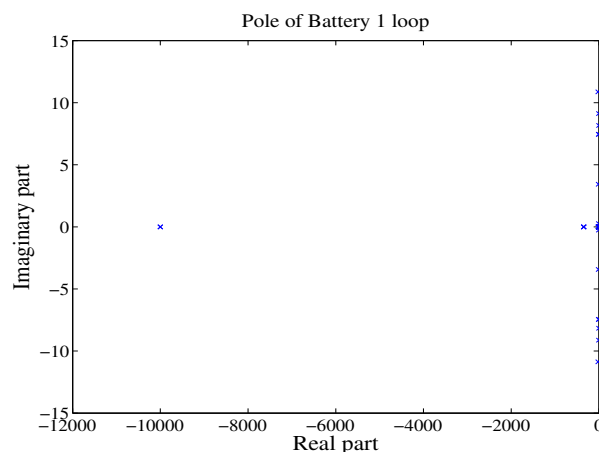
7.5. Examination of the Simulation Results for Real Whole Day Data of Okinawa, Japan

The effectiveness and robustness of the proposed scheme is investigated using actual solar radiation and wind speed of Okinawa, Japan in this case study. The Japan Weather Association (JWA) [38] is used to get these actual data. Full day 24 h actual data are used in this study. Moreover,

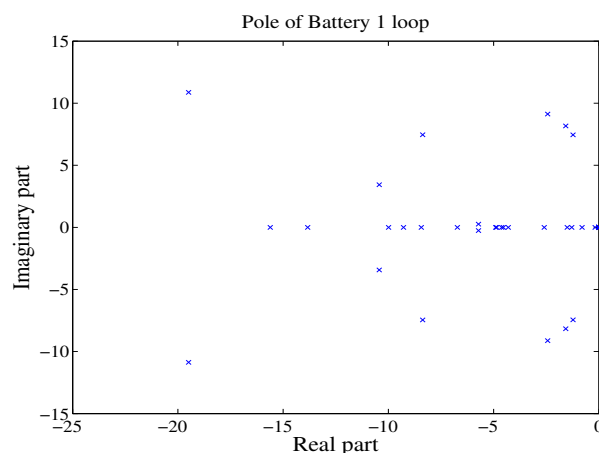
all of storage battery, RES and demand response control schemes are considered in this case study. The associated simulation results are then presented in Figure 20. Simulation results show the ability of the proposed control scheme to modify the load at each bus depending on frequency deviation value as shown in Figure 20b. Accordingly, mismatch between generation and demand can be mitigated and frequency fluctuation can be suppressed as shown in Figure 20a,d, respectively. Moreover, Figure 20e–h confirm the capability of the proposed technique to control storage battery and thermal generators active powers and keep their SOC and operation ratio, respectively within the permissible values. Furthermore, the proposed approach succeeded to keep the buses voltage near to $1 pu$ without violating the allowable range. Even with this harsh real operating conditions as shown in Figure 20l,m. Finally, the real solar radiation and wind speed for whole day 24-h case study with their associated RES output powers are shown in Figure 20n,o,i,j, respectively.

7.6. Stability Evaluation of Each Controller

In the case of introducing storage batteries, renewable energy generators, and demand response, we evaluate the stability of each controller. In stability evaluation, we calculate poles of each control loop and to see if the real part of the pole is negative value to judge the stability. Moreover, zoomed pole map for every control loop is presented to make it easier for the reader to investigate the poles values near origin. In Figures 21–27, since the real part of the poles in the control loop of each system are all negative values, the control system is stable.

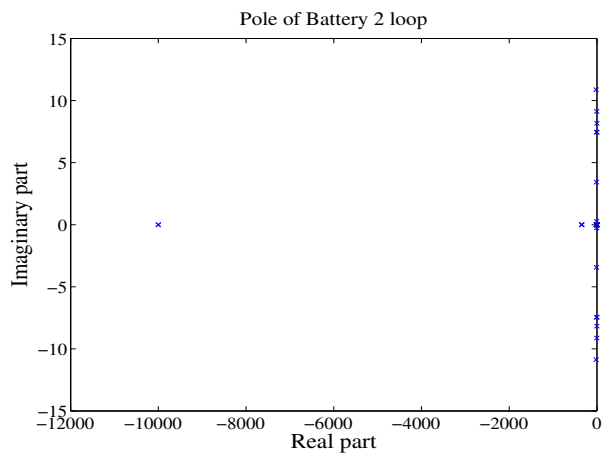


(a) Pole map for the control loop of the battery 1

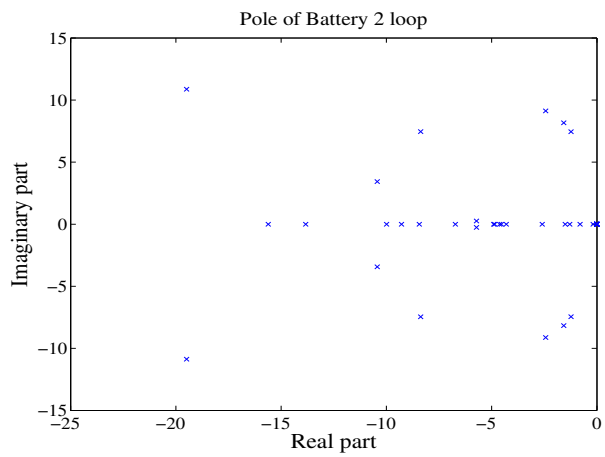


(b) Zoomed pole map pole for the control loop of the battery 1

Figure 21. Pole map for the control loop of the battery 1.

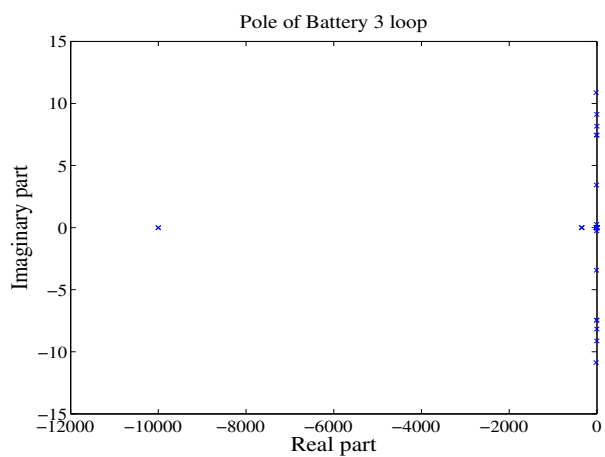


(a) Pole map for the control loop of the battery 2



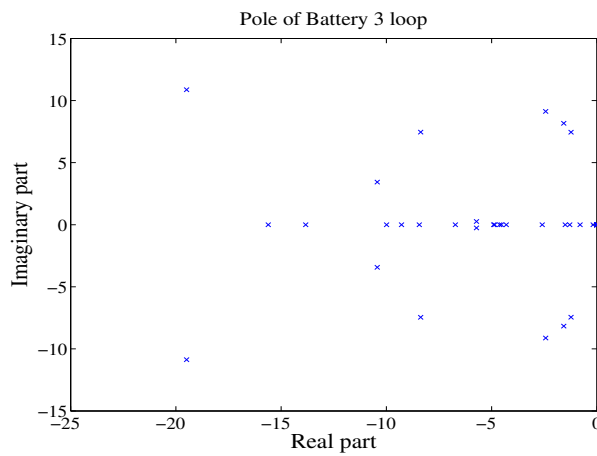
(b) Zoomed pole map for the control loop of the battery 2

Figure 22. Pole map for the control loop of the battery 2.



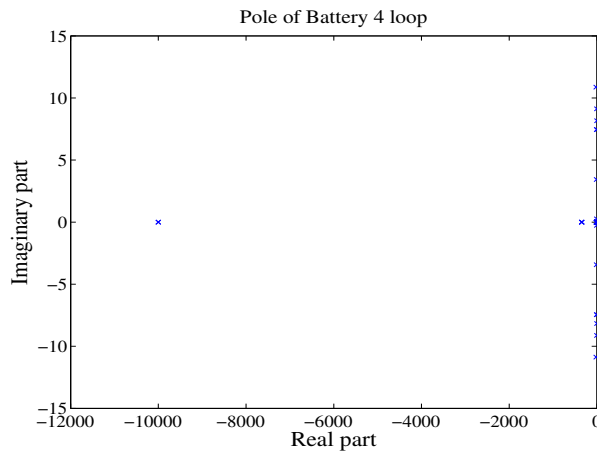
(a) Pole map for the control loop of the battery 3

Figure 23. Cont.

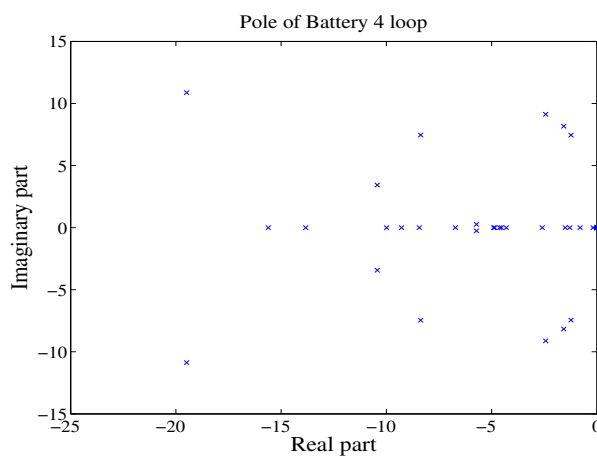


(b) Zoomed pole map pole for the control loop of the battery 3

Figure 23. Pole map for the control loop of the battery 3.



(a) Pole map for the control loop of the battery 4



(b) Zoomed pole map for the control loop of the battery 4

Figure 24. Pole map for the control loop of the battery 4.

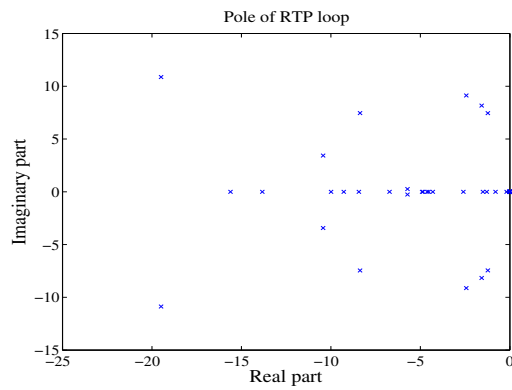
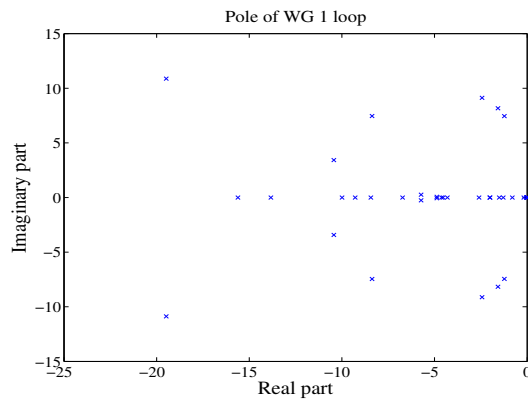
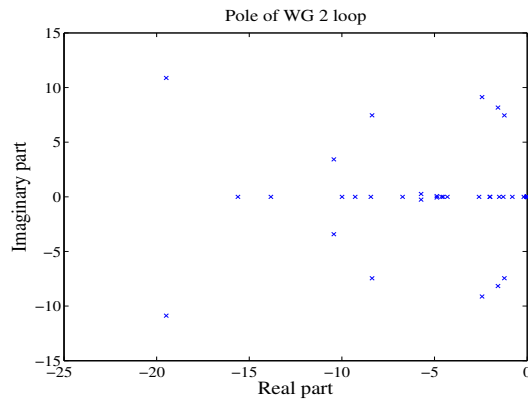


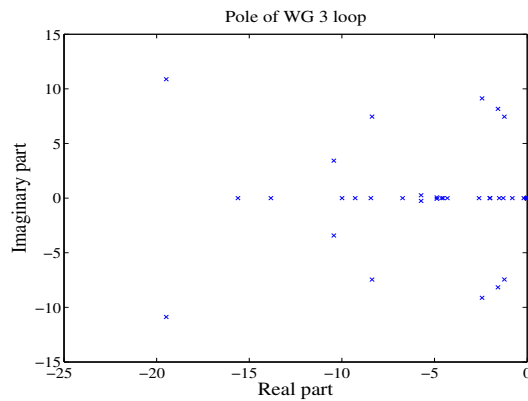
Figure 25. Pole map for the RTP loop at a point near the coordinate origin.



(a) Pole map for the control loop pf the WG 1 at a point near the coordinate origin

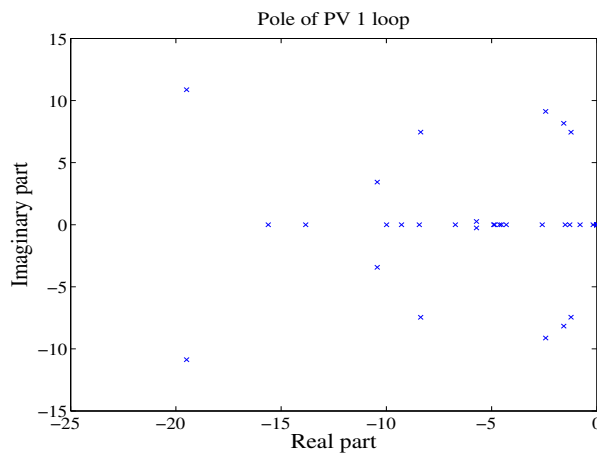


(b) Pole map for the control loop pf the WG 2 at a point near the coordinate origin

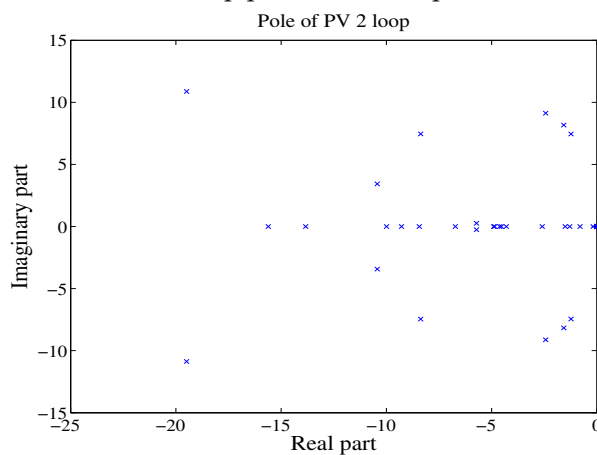


(c) Pole map for the control loop pf the WG 3 at a point near the coordinate origin

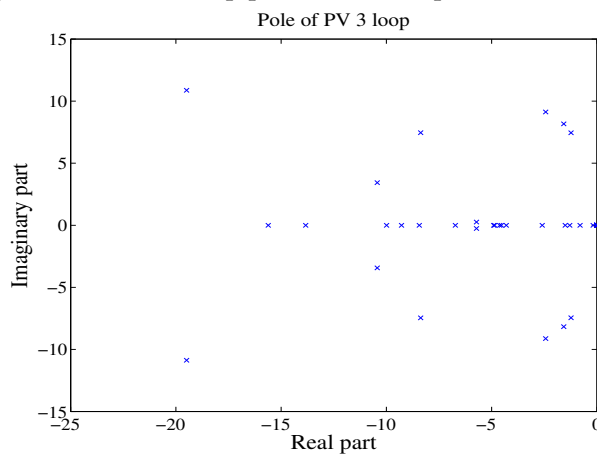
Figure 26. Pole map for the control loop of each WG.



(a) Pole map for the control loop pf the PV 1 at a point near the coordinate origin



(b) Pole map for the control loop pf the PV 2 at a point near the coordinate origin



(c) Pole map for the control loop pf the PV 3 at a point near the coordinate origin

Figure 27. Pole map for the control loop of each PV.

8. Conclusions

A modern output power control approach for small-scale power system has been discussed in this research. Adorable RES output control scheme is presented that combines MPPT technique and output power suppression mechanism depending on the value of frequency fluctuations. Three case studies with their detailed analysis are considered in this research for output power control using storage battery, RES, and real-time price demand response. Moreover, fourth scenario is presented with whole one day simulation data of Okinawa island, Japan, to confirm the robustness and effectiveness of the

proposed control scheme. The real 10-bus power system model of Okinawa island, Japan is used to investigate the performance of the intended control technique. Furthermore, the stability of all control loops are checked using pole-zero maps. The simulation results for the four scenarios confirms the ability of the proposed control scheme to control the loads at each bus so as to minimize the mismatch between generation and demand and accordingly suppress the frequency fluctuations. Moreover, the proposed control approach succeeded to keep the buses voltage, batteries state of charge and thermal generation operation ratios within their permissible ranges even under different operating conditions. Overall, the performance of the power system is enhanced significantly using the proposed control approach. Extending this study to analyze the performance of the hybrid power system with other types of controllable loads such as electric vehicle with Vehicle-to-Grid (V2G) application, using additional types of demand response techniques, and utilizing different control schemes such as model predictive control (MPC) and H_∞ is the subsequent task in the near future to make the related study results further solid and practical.

Author Contributions: All authors contributed to this work. L.L., H.M., and M.E.L. performed the research, discussed the results, and prepared the manuscript. M.D. and T.S. suggested the idea, and contributed to writing and revising the paper. All authors revised and approved the manuscript.

Funding: This research received no external funding.

Conflicts of Interest: The authors declare no conflict of interest.

Abbreviations

The following abbreviations are used in this manuscript:

V_{pv}	Photovoltaic output voltage
P_{pv}	Photovoltaic output power
V_{pv_mptt}	Output voltage command value
Δf	Load frequency deviation
k	Control weight
b	Pitch angle command value of wind turbine generator
f	Load frequency
f_{ref}	Reference frequency
π	Power price
V_{wg}	Wind turbine generator voltage
P_{wg}	Wind turbine generator power

References

1. Stott, P.A.; Mueller, M.A. Modelling fully variable speed hybrid wind diesel systems. In Proceedings of the 41st International Universities Power Engineering Conference, Newcastle upon Tyne, UK, 6–8 September 2006.
2. Alternative Energy Solutions for the 21st Century, Renewable Energy. Available online: <http://www.altenergy.org/renewables/renewables.html> (accessed on 6 November 2018).
3. Siano, P. Demand response and smart grid—A survey. *Renew. Sustain. Energy Rev.* **2014**, *30*, 461–478. [[CrossRef](#)]
4. Kim, A.R.; Seo, H.R.; Kim, G.H.; Park, M.W.; Yu, I.K.; Otsuki, Y.; Tamura, J.; Kim, S.-H.; Sim, K.; Seong, K.C. Operating characteristic analysis of HTS SMES for frequency stabilization of dispersed power generation system. *IEEE Trans. Appl. Supercond.* **2010**, *20*, 1334–1338.
5. Bevrani, H.; Habibi, F.; Babahajyani, P.; Watanabe, M.; Mitani, Y. Intelligent Frequency Control in an AC Microgrid: Online PSO-Based Fuzzy Tuning Approach. *IEEE Trans. Smart Grid* **2012**, *3*, 1935–1944. [[CrossRef](#)]
6. Pandiaraj, K.; Taylor, P.; Jenkins, N.; Robb, C. Distributed load control of autonomous renewable energy systems. *IEEE Trans. Energy Convers.* **2001**, *16*, 14–19. [[CrossRef](#)]
7. Moghadam, M.R.V.; Ma, R.T.; Zhang, R. Distributed Frequency Control in Smart Grids via Randomized Demand Response. *IEEE Trans. Smart Grid.* **2014**, *5*, 2798–2809. [[CrossRef](#)]

8. Medina, J.; Muller, N.; Roytelman, I. Demand Response and Distribution Grid Operations: Opportunities and Challenges. *IEEE Trans. Smart Grid*. **2010**, *1*, 193–198. [[CrossRef](#)]
9. Navid-Azarbaijani, N.; Banakar, M.H. Realizing load reduction functions by aperiodic switching of load groups. *IEEE Trans. Power Syst.* **1996**, *11*, 721–727. [[CrossRef](#)]
10. *Benefits of Demand Response in Electricity Markets and Recommendations for Achieving Them: A Report to U.S. Congress*; US Department Energy: Washington, DC, USA, 2006.
11. Samarakoon, K.; Ekanayake, J.; Jenkins, N. Investigation of Domestic Load Control to Provide Primary Frequency Response Using Smart Meters. *IEEE Trans. Smart Grid* **2012**, *3*, 282–292. [[CrossRef](#)]
12. Mercier, P.; Cherkaoui, R.; Oudalov, A. Optimizing a battery energy storage system for frequency control application in an isolated power system. *IEEE Trans. Power Syst.* **2009**, *24*, 1469–1477. [[CrossRef](#)]
13. Hatziargyriou, H.; Kanellos, F.; Kariniotakis, G.; Le Pivert, X.; Jenkins, N.; Jayawarna, N. *Modeling of Micro-Sources for Security Studies*; CIGRE Session: Paris, France, 2004.
14. Oudalov, A.; Chartouni, D.; Ohler, C.; Linhofer, G. Value analysis of battery energy storage applications in power systems. In Proceedings of the 2006 IEEE PES Power Systems Conference and Exposition, Atlanta, GA, USA, 29 October–1 November 2006; pp. 2206–2211.
15. Aditya, S.K.; Das, D. Application of battery energy storage system to load frequency control of an isolated power system. *Int. J. Energy Res.* **1999**, *23*, 247–258. [[CrossRef](#)]
16. Oudalov, A.; Chartouni, D.; Ohler, C. Optimizing a battery energy storage system for primary frequency control. *IEEE Trans. Power Syst.* **2007**, *22*, 1259–1266. [[CrossRef](#)]
17. Babahajiani, P.; Shafiee, Q.; Bevrani, H. Intelligent Demand Response Contribution in Frequency Control of Multi-area Power Systems. *IEEE Trans. Smart Grid* **2018**, *9*, 1282–1291. [[CrossRef](#)]
18. Dehghanpour, K.; Afsharnia, S. Electrical demand side contribution to frequency control in power systems: a review on technical aspects. *Renew. Sustain. Energy Rev.* **2015**, *41*, 1267–1276. [[CrossRef](#)]
19. Rezaei, N.; Kalantar, M. Stochastic frequency-security constrained energy and reserve management of an inverter interfaced islanded microgrid considering demand response programs. *Int. J. Elect. Power Energy Syst.* **2015**, *69*, 273–286. [[CrossRef](#)]
20. Rezaei, N.; Kalantar, M. Smart microgrid hierarchical frequency control ancillary service provision based on virtual inertia concept: An integrated demand response and droop controlled distributed generation framework. *Energy Convers. Manag.* **2015**, *92*, 287–301. [[CrossRef](#)]
21. Molina-Garcia, A.; Munoz-Benavente, I.; Hansen, A.D.; Gomez-Lazaro, E. Demand-Side Contribution to Primary Frequency Control with Wind Farm Auxiliary Control. *IEEE Trans. Power Syst.* **2014**, *29*, 2391–2399. [[CrossRef](#)]
22. Jiang, H.; Lin, J.; Song, Y.; Gao, W.; Xu, Y.; Shu, B.; Li, X.; Dong, J. Demand Side Frequency Control Scheme in an Isolated Wind Power System for Industrial Aluminum Smelting Production. *IEEE Trans. Power Syst.* **2014**, *29*, 844–853. [[CrossRef](#)]
23. Gouveia, C.; Moreira, J.; Moreira, C.L.; Pecas Lopes, J.A. Coordinating Storage and Demand Response for Microgrid Emergency Operation. *IEEE Trans. Smart Grid* **2013**, *4*, 1898–1908. [[CrossRef](#)]
24. Pourmousavi, S.A.; Nehrir, M.H. Introducing Dynamic Demand Response in the LFC Model. *IEEE Trans. Power Syst.* **2014**, *29*, 1562–1572. [[CrossRef](#)]
25. Angeli, D.; Kountouriotis, P.A. A Stochastic Approach to “Dynamic-Demand” Refrigerator Control. *IEEE Trans. Control Syst. Technol.* **2012**, *20*, 581–592. [[CrossRef](#)]
26. Hao, H.; Fangxing, L. Sensitivity Analysis of Load-Damping Characteristic in Power System Frequency Regulation. *IEEE Trans. Power Syst.* **2013**, *28*, 1324–1335.
27. Weckx, S.; D’Hulst, R.; Driesen, J. Primary and Secondary Frequency Support by a Multi-Agent Demand Control System. *IEEE Trans. Power Syst.* **2015**, *30*, 1394–1404. [[CrossRef](#)]
28. Short, J.A.; Infield, D.G.; Freris, L.L. Stabilization of Grid Frequency Through Dynamic Demand Control. *IEEE Trans. Power Syst.* **2007**, *22*, 1284–1293. [[CrossRef](#)]
29. Chang-Chien, L.R.; An, L.N.; Lin, T.W.; Lee, W.J. Incorporating Demand Response With Spinning Reserve to Realize an Adaptive Frequency Restoration Plan for System Contingencies. *IEEE Trans. Smart Grid* **2012**, *3*, 1145–1153. [[CrossRef](#)]
30. Zhao, X.; Ostergaard, J.; Togeby, M. Demand as Frequency Controlled Reserve. *IEEE Trans. Power Syst.* **2011**, *26*, 1062–1071.

31. Douglass, P.J.; Garcia-Valle, R.; Nyeng, P.; Ostergaard, J.; Togeby, M. Smart Demand for Frequency Regulation: Experimental Results. *IEEE Trans. Smart Grid* **2013**, *4*, 1713–1720. [[CrossRef](#)]
32. Changhong, Z.; Topcu, U.; Low, S.H. Optimal Load Control via Frequency Measurement and Neighborhood Area Communication. *IEEE Trans. Power Syst.* **2013**, *28*, 3576–3587.
33. Tavakkoli, M.; Adabi, J.; Zabihi, S.; Godina, R.; Pouresmaeil, E. Reserve Allocation of Photovoltaic Systems to Improve Frequency Stability in Hybrid Power Systems. *Energies* **2018**, *11*, 2583. [[CrossRef](#)]
34. Tavakoli, M.; Pouresmaeil, E.; Adabi, J.; Godina, R.; Catalao, J.P. Load-Frequency Control in a Multi-Source Power System Connected to Wind Farms through Multi Terminal HVDC Systems. *Comput. Oper. Res.* **2018**, *96*, 305–315. [[CrossRef](#)]
35. Tavakoli, M.; Shokridehaki, F.; Marzband, M.; Godina, R.; Pouresmaeil, E. A Two Stage Hierarchical Control Approach for the Optimal Energy Management in Commercial Building Microgrids Based on Local Wind Power and PEVs. *Sustain. Cities Soc.* **2018**, *41*, 332–340. [[CrossRef](#)]
36. Lotfy, M.E.; Senjyu, T.; Farahat, M.A.-F.; Abdel-Gawad, A.F.; Yona, A. A Frequency Control Approach for Hybrid Power System Using Multi-Objective Optimization. *Energies* **2017**, *10*, 80. [[CrossRef](#)]
37. Lotfy, M.E.; Senjyu, T.; Farahat, M.A.-F.; Abdel-Gawad, A.F.; Lei, L.; Datta, M. Hybrid Genetic Algorithm Fuzzy-Based Control Schemes for Small Power System with High-Penetration Wind Farms. *Appl. Sci.* **2018**, *8*, 373. [[CrossRef](#)]
38. The Japan Weather Association. Available online: <http://www.jwa.or.jp/english> (accessed on 28 June 2017).



© 2018 by the authors. Licensee MDPI, Basel, Switzerland. This article is an open access article distributed under the terms and conditions of the Creative Commons Attribution (CC BY) license (<http://creativecommons.org/licenses/by/4.0/>).